This is a repository copy of *Feasibility study on a full-scale wind turbine blade monitoring campaign: Comparing performance and robustness of features extracted from medium-frequency active vibrations*.

White Rose Research Online URL for this paper:
https://eprints.whiterose.ac.uk/202426/

Version: Published Version

RESEARCH ARTICLE

WILEY

Feasibility study on a full-scale wind turbine blade monitoring campaign: Comparing performance and robustness of features extracted from medium-frequency active vibrations

M. A. Fremmelev[1,2] | P. Ladpli[1] | E. Orlowitz[3] | N. Dervilis[4] | M. McGugan[2] | K. Branner[2]

[1]Blade Submodules Technology, Siemens Gamesa Renewable Energy, Aalborg East, Denmark

[2]Department of Wind and Energy Systems, Technical University of Denmark, Roskilde, Denmark

[3]Turbine Measurement Operation, Siemens Gamesa Renewable Energy, Brande, Denmark

[4]Dynamics Research Group, Department of Mechanical Engineering, University of Sheffield, Sheffield, United Kingdom

Correspondence
M. A. Fremmelev, Blade Submodules Technology, Siemens Gamesa Renewable Energy, Assensvej 11, 9220 Aalborg East, Denmark.
Email: mads.fremmelev@siemensgamesa.com

Present Address
Assensvej 11, 9220 Aalborg East, Denmark.

Funding information
Energistyrelsen, Grant/Award Number: 64018-0068; Innovationsfonden, Grant/Award Number: 9065-00200B; Innovation Fund Denmark, Grant/Award Number: 9065-00200B; Energy Technology Development and Demonstration Program (EUDP), Grant/Award Number: 64018-0068

Abstract

The present work investigates the performance of different features, extracted from vibration-based data, for structural health monitoring of a 52-meter wind turbine blade during fatigue testing. An active vibration monitoring system was used during the test campaign, providing periodic excitation of single frequencies in the medium-frequency range, and using accelerometers to measure the vibration output on different parts of the blade. Based on previous work from the authors, data is available for the wind turbine blade in healthy state, with a manually induced damage, and with progressively increasing damage severity. Using the vibration data, different signal processing methods are used to extract damage-sensitive features. Time series methods and time-frequency domain methods are used to quantify the applied active vibration signal. Using outlier analysis, the health state of the blade is classified, and the classification accuracy through use of the different features is compared. Highest performance is generally obtained by auto-regressive modeling of the vibration outputs, using the auto-regressive parameters as features. Finally, suggestions for future improvements of the present method toward practical implementation are given.

KEYWORDS
active vibration input, damage, feature selection, outlier detection, structural health monitoring, wind turbine blades

1 | INTRODUCTION

Operations and maintenance costs of offshore wind turbines are expected to reach €11 billion by 2028.[1] One of the most costly components in terms of repairs and its contribution to downtime is wind turbine blades.[2,3] Being large components manufactured from fiber reinforced polymer composites, manufacturing defects are inherent, and these may develop into severe damages over the life of the turbines.[4-6] Today, the structural integrity of wind turbine blades is most commonly determined through interval-based inspections. This is a costly and time-consuming process, which only gives information on the health state of blades in a snapshot in time with each manual inspection. A possible alternative to interval-based inspections in the form of sensor-based structural health monitoring (SHM) has gained increasing popularity in the research community,

due to its prospect of enabling continuous automated monitoring of structures. This would reduce or even remove the need for scheduled manual inspections, and facilitate a transition toward predictive maintenance, where manual inspections are only performed based on informed suspicions of a structure being damaged.

Sensor-based SHM methods rely on measurements collected over the life of a structure, using signal processing methods to detect changes in the structural response resulting from damage. As such, it is not necessarily required to have a model of the structure in question, and instead focus may be put on selection of appropriate sensing systems and signal processing algorithms, which may enable reliable SHM.

In the past decades, much work has been done toward investigations of wind turbine SHM, and the use of various sensing systems for SHM of different parts of wind turbines, including blades, has been reviewed.[7-14] These reviews have shown that vibration-based sensing systems represent a viable option for blade SHM, due to their comparatively low system cost, straight-forward installation, high maturity, and potentially high sensitivity to damages. To minimize turbine downtime, caused by blade damage, damages need to be detected and contained at an early stage, before they grow to a critical size, requiring costly and time-consuming down-tower repairs or even replacements with new blades.

Vibration-based methods span from the low-frequency range, for natural vibration modes of wind turbine blades,[15-18] to the high-frequency range for acoustic emission (AE)[18-20] and guided waves.[21-26] Common for vibration-based methods, regardless of the frequency range, is that they rely on detection of changes in the vibration response of structures. To facilitate this, damage-sensitive features need to be extracted from the recorded time-series vibration data, which does not in itself serve as a reliable indicator for damage due to inherent randomness in time series data.[27] Signal processing methods used for extraction of features from vibration-based data have been reviewed,[28,29] commonly being split into two categories: time-domain and frequency-domain techniques, respectively. Time-domain-based damage-sensitive features are e.g., statistical measures[13] and auto-regressive (AR) parameters,[30] with the latter being commonly applied to stochastic time-series signals. Frequency-domain methods used for feature extraction are e.g., the short-time Fourier transform[31] and the wavelet transform.[32-34]

Generally, the wavelength of a vibration signal is proportionate to the detectable dimension of damage, i.e. detection of small damages requires small wavelengths and thereby high-frequency vibrations. In the low-frequency range, monitoring of large structures is commonly concerned with global modal parameters, being natural frequencies, mode shapes, and damping estimates. Vibration-based methods relying on monitoring of low-frequency natural vibrations of wind turbine blades are insensitive for detection of small damages.[18,35,36] For low-frequency natural vibration modes to serve as reliable features for SHM, damages need to affect the global stiffness of the structure. For the case of wind turbine blades, a damage that affects the global stiffness sufficiently to cause detectable changes in modal parameters will be of a size that requires extensive repair, very likely being close to resulting in failure of the blade. Thus, monitoring of low-frequency modal parameters is not deemed to be ideal in terms of minimizing downtime and repair costs.

In the high-frequency range, say above 10 kHz, local vibration properties are monitored, with a significant factor affecting performance being the high attenuation of high-frequency vibrations in fiber reinforced polymer composites. AE sensors are useful for monitoring localized high-frequency vibrations caused by damage propagation. Similarly, guided waves systems are useful for detection of damages through monitoring the local response of a high-frequency vibration input signal. Common for monitoring systems using the high-frequency range is their limited range, requiring a high number of sensors for monitoring of an entire wind turbine blade.[37]

Based on the cited literature, low- and high-frequency vibration systems have opposing advantages and drawbacks concerning useful detection range and sensitivity to damage size. To enable monitoring of large areas with a limited number of sensors, while obtaining sensitivity to small damages, it would thus be reasonable to seek a compromise between these two ends of the frequency range. This is done by focusing on vibrations in the medium-frequency range, being somewhere between the low- and high-frequency range. The medium-frequency range is not excited sufficiently through ambient excitation from e.g. wind,[38] and frequencies emitted by propagating damages are, as mentioned previously, in the high-frequency range. Thus, it is necessary to provide an active vibration input in the frequency range of interest.

The use of the medium-frequency range, providing an active vibration excitation, has been investigated, resulting in a good compromise between detectable damage size and detection distance.[38-42] An electromechanical actuator was used to apply active vibration excitation to wind turbine blades, providing a high signal-to-noise ratio in the medium-frequency range. The proposed system proved to be robust to noise as well as variations in environmental conditions during use on a blade of an operating wind turbine.

Our previous work investigated the use of an electrodynamic vibration shaker for excitation with active vibrations in the medium-frequency range for wind turbine blade SHM. Using accelerometer outputs, the power spectral density estimate was selected as a feature for detection of damage initiation and propagation.[18,43] A 52-meter wind turbine blade was used for studying the utilization of the active vibration monitoring system. Different damages were manually introduced in the blade laminate, and fatigue testing was performed to propagate the lengths of the damages, recording data over the course of the test campaign. With the electrodynamic vibration shaker, a swept sine signal with logarithmic increase in frequency was applied at frequencies between 100 and 3,000 Hz. The frequency range useful for detection of the introduced damages was found to be between 600 and 2,500 Hz with the given electrodynamic shaker, taking into account the noise present during fatigue testing, which decreased significantly in magnitude at frequencies above 600 Hz.

This work extends our previous studies, investigating the use of single-frequency active vibration input signals, using different signal processing methods to extract features, and comparing their damage sensitivity. Furthermore, performance in outlier detection using these

features is compared. The previously mentioned 52-meter commercial wind turbine blade is used, subjected to fatigue testing and investigating the detection of initiation and propagation of a shear web crack.

Using the electrodynamic shaker, a sinusoidal signal with a Gaussian envelope is applied in the medium-frequency range, using accelerometers to measure the vibration output at different parts of the wind turbine blade. With the present work being a feasibility study on a full-scale wind turbine blade test campaign, method development is in focus. Thus, it has not been attempted to develop new features. Instead, a practical study is conducted, investigating how medium-frequency vibration features perform in detection of real damages in a large wind turbine blade. As such, well-known existing features are chosen and tested in an industrial environment on an actual wind turbine blade. Thus, it has not been attempted to develop new features, but instead, a practical study is conducted, investigating how medium-frequency vibration features perform in detection of real damages in a large wind turbine blade. As such, well-known existing features are chosen and tested in an industrial environment on an actual wind turbine blade. Toward this goal, the following signal processing methods are used to extract damage-sensitive features: AR modeling, extraction of statistical measures, and extraction of the time-frequency domain response. Through the used signal processing methods, features sensitive to changes in the local vibration response are extracted, enabling detection of initiation of the shear web crack, and progressive damage growth during fatigue testing is tracked. While the method proves to be successful in detection and monitoring of damage, the dependency on the frequency response changing at the specific input frequencies is discussed.

The conducted blade test, the investigated damage case, and the used signal processing methods for detection of damage initiation and progression are presented in Section 2. Results from the data analysis are presented in Section 3, showing the capabilities and limitations of the used active vibration monitoring system and signal processing methods for structural health monitoring of wind turbine blades. Section 4 includes discussions on the used sensing system and signal processing methods, and Section 5 provides conclusions for the findings of this work.

2 | METHODS

Toward the design of an SHM system for wind turbine blades, an extensive blade test campaign was conducted at the Siemens Gamesa Renewable Energy Blade Test Center in Aalborg, Denmark, as previously documented by the authors.[18,43]

The present test campaign is, at the time of writing, one of a kind targeted toward detection of damages in blades, stemming from the use of a large, commercial wind turbine blade, multiple damage cases, including intermediate repair of damages, and the simultaneous use of well-established as well as novel sensing systems. The blade test campaign spanned eight months, where both flapwise and edgewise fatigue testing was conducted. A total of four artificial damages were simulated through manual introduction in the blade laminate, all being representative of damages that could be expected in blades on an operating turbine. To enable studies on blade SHM, various sensing systems were used to record data during the blade test. From our previous work, it was found that obtaining progressive development of the manually induced damages during fatigue testing proved challenging, requiring larger damages than first assumed. Furthermore, it was found that most of the investigated sensing systems proved useful for blade SHM; either by enabling localized monitoring, or, in the case of the active vibration monitoring system, enabling monitoring within large areas.

The active vibration monitoring system, which will be presented in Section 2.3, received particular attention from the authors since initial results showed great promise for such a system targeted toward blade SHM. Additionally, an active vibration monitoring system is of great interest, since its practical application in blades on operating turbines could be achieved through e.g., active flaps or blade pitching. Thus, the present work is concerned with method development within the use of active vibration monitoring systems for blade SHM, using both classical features and methods for outlier analysis, through which the great promise of this type of SHM system is showcased.

The following includes a short overview of the test campaign, the sensing system used for this work, and the simulated damage case.

2.1 | Blade test

The wind turbine blade used in the conducted test is shown in Figure 1, being a 52-meter commercial blade mounted pressure side up on a concrete foundation. The blade was tested inside a temperature-controlled hall, and changes in environmental conditions, such as temperature, were thus eliminated. Furthermore, boundary conditions in terms of root bolts and loading saddle for the rotating mass fatigue exciter were not altered for the data considered in this paper. Consequently, any changes discovered in the structural response of the blade through the collected data are deemed to be resulting from the induced damage.

Cyclic fatigue testing was conducted in the flapwise direction at the first eigenfrequency of the blade using a rotating mass exciter. The purpose of the test was to gain understanding of progressive damage development in wind turbine blades and to collect data that would enable studies on blade SHM. Data was collected both during fatigue testing and during periods of no excitation applied to the blade with the fatigue exciter, which is denominated stand-still in this work. During fatigue testing, the amplitude of ambient noise was at a much higher level than during stand-still. Thus, data is available for two different operational states, enabling studies on the robustness of the proposed method for blade SHM.
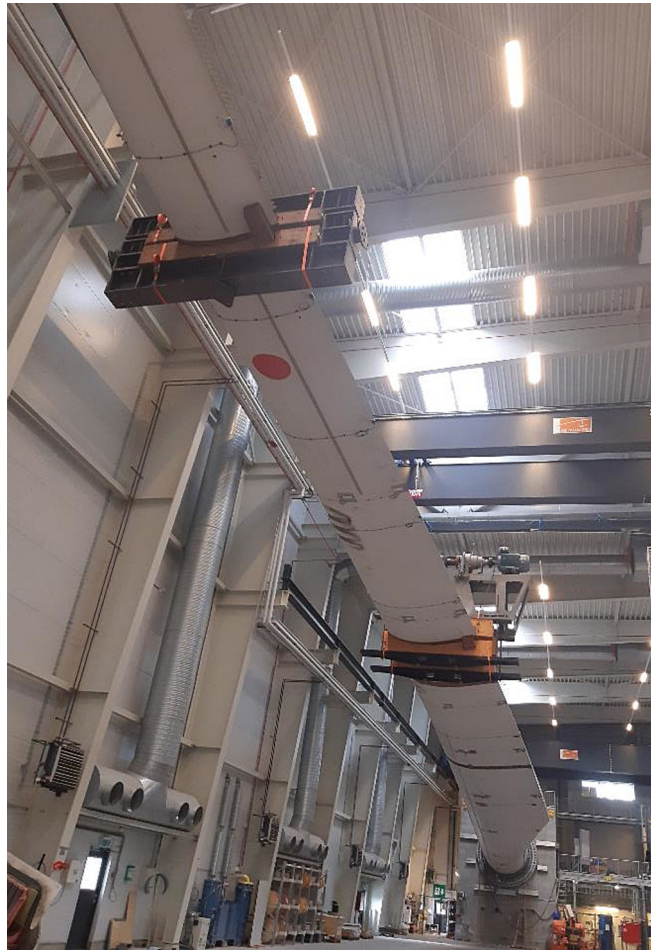
FIGURE 1   Wind turbine blade mounted on a concrete foundation at Siemens Gamesa Blade Test Center in Aalborg, Denmark.

2.2 | Manually induced damage

The blade used for this work was manually inspected at the beginning of the test campaign, and no visible damage was found. To enable studies on blade SHM, a damage was simulated by manually cutting through the whole thickness of the shear web laminate for a length of 100 mm at spanwise position 7.5 meters. Following the manual introduction of the damage, fatigue testing was conducted to propagate the damage. Thus, data was available for the healthy state of the blade, the damaged state of the blade after manual introduction, and with progressively increasing damage severity over the course of the fatigue test. Figure 2(A) shows part of the shear web laminate with the manually induced damage, Figure 2(B–C) shows the crack propagating over the course of the fatigue test, and Figure 2(D) shows the final damage size, which was obtained when testing was stopped. At this point, the crack had propagated through the shear web to the spar cap laminate. Delaminations had also formed in the shear web laminate and in the spar cap laminate over the course of the fatigue test. The location of the shear web damage is shown in Figure 4(A).

2.3 | Active vibration system for blade structural health monitoring

The authors previously described a sensing system for blade SHM, applying active medium-frequency vibration excitation to the blade.[18] This active vibration monitoring system, see Figure 3, consists of an electrodynamic vibration shaker (Dewesoft DS-IS-40) with a frequency range of 10 - 3,000 Hz, a colocated force transducer (Dytran 1053V1), as well as 11 uniaxial accelerometers (Brüel & Kjær type 4507-B-006) with a frequency range of 0.2 - 6,000 Hz, mounted with the measurement direction normal to the blade surface. The force transducer, which measured force normally to the blade surface, was mounted with a steel base plate, adhered to the blade surface, and the vibration shaker was mounted in line with the force transducer. Screw connections with threadlock adhesive were used to connect the steel base plate, force transducer, and vibration shaker. The accelerometers were mounted with plastic clips, also adhered to the blade surface. An NI cDAQ-9185 data acquisition unit with
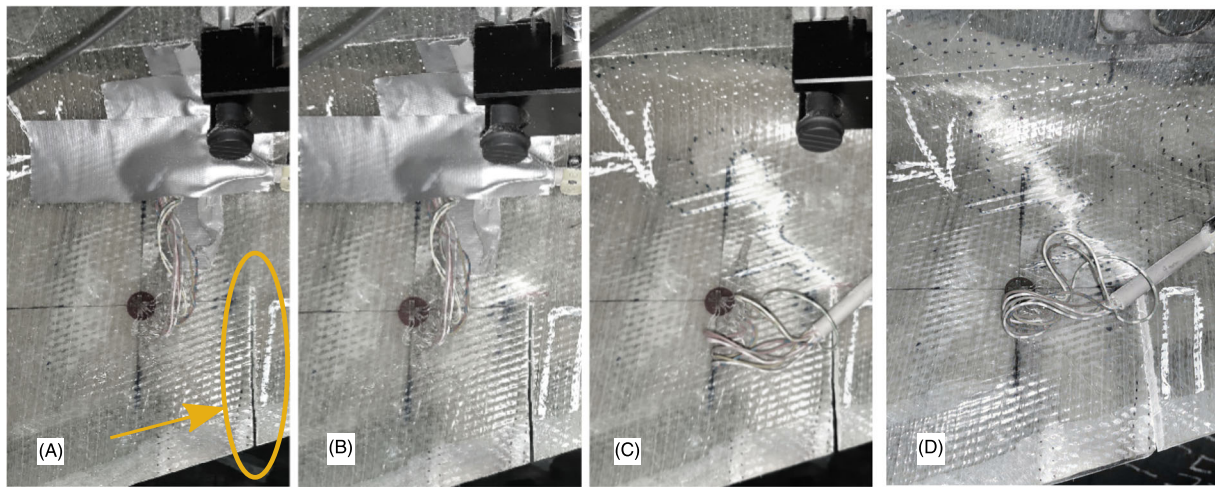
FIGURE 2   Manually induced shear web damage (marked with orange ellipsis) (A), followed by fatigue-driven damage propagation (B-C), and final damage size when fatigue testing was stopped (D). Delaminations developed from the induced crack, manually marked with dots.
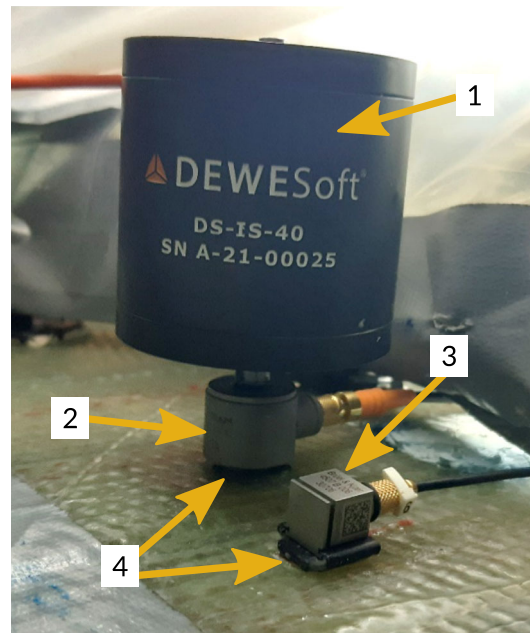

FIGURE 3   Electrodynamic vibration shaker (1) mounted on shear web laminate inside the wind turbine blade, force transducer colocated with the vibration shaker (2), accelerometer (3), and mounting plates (4).

an NI-9260 output module and three NI-9234 input modules was used for signal generation and data acquisition, controlled through a laptop PC with MATLAB software. A sampling frequency of 25,600 Hz was used for the force transducer and the accelerometers.

The locations of the vibration shaker, accelerometers, and damage are sketched in Figure 4(A). The vibration shaker was placed on the shear web laminate to obtain good excitation of the laminate in which the damage was located. The sensor locations were chosen based on engineering judgment, investigating feasibility for damage detection on different parts of the blade laminate. Accelerometers were placed on the web laminate (white boxes) as well as on the shell laminate toward the trailing edge (blue boxes), see Figure 4(B) for a sketch of the cross-sectional view of the sensor locations.

Using the vibration shaker, sinusoidal signals with single frequencies of $f = [750\ 1,000\ 1,250\ 1,500\ 2,000]$ Hz were applied one at a time, repeated periodically over the course of the blade test campaign. The sinusoidal signals were applied for a duration of two seconds, applying a Gaussian envelope to the amplitude of the vibration input. Thus, the time dependence of the amplitude can be tracked, and changes in this distribution may be indicative of the presence of damage in the blade. A total of 5,614 observations are available for each of the input frequencies, of which 3,081 are in the healthy state and 2,534 are in the damaged state, i.e. before and after manual introduction of the damage, respectively.
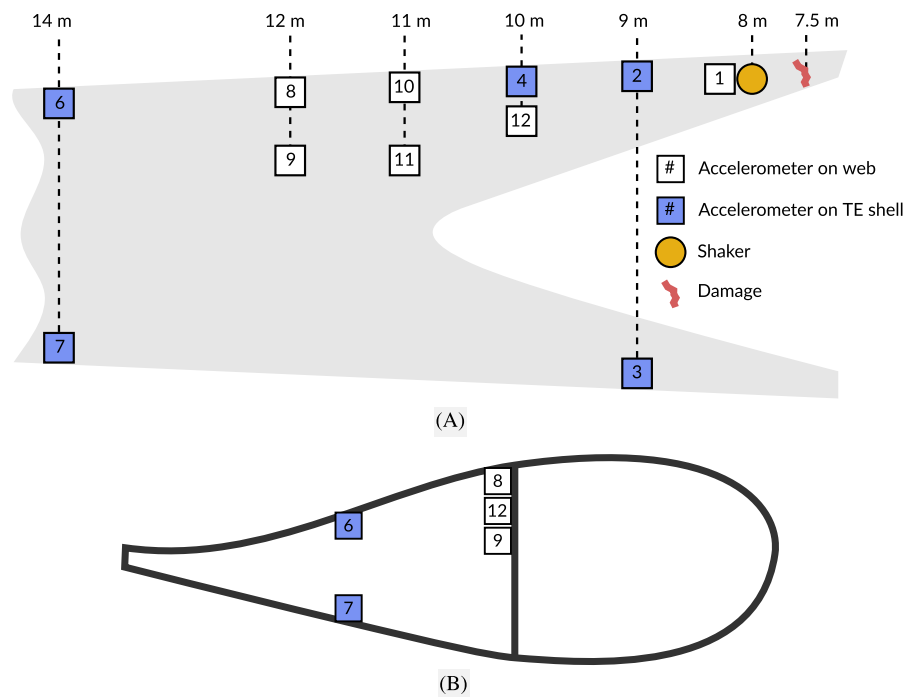
FIGURE 4 (A): Accelerometer placement on shear web and shell laminate, viewed from trailing edge side. The shear web damage is shown in Figure 2. (B): Cross-sectional view of the blade seen from the root end, showing accelerometer placement on the shear web and shell laminate. The shown sensor channels are not physically placed at the same spanwise position, see (A) for the spanwise placement of the sensors. Drawings are not to scale.

The input from the vibration shaker, measured with the force transducer during stand-still, is plotted in Figure 5(A), showing the active vibration input being applied at 1 s, with a peak amplitude at 2 s, end of the active signal at 3 s, and a period of 1 s with no active input at both ends of the signal. The spectrogram of force transducer time series data is plotted in Figure 5(B), showing the input signal frequency of 2,000 Hz. Similarly, the output measurement from accelerometer 9, measured during stand-still, see Figure 4, is plotted in Figure 5(C), with the associated spectrogram shown in Figure 5(D). During fatigue testing, the noise level is much higher, as plotted in Figure 5(E), showing the output measurement from accelerometer 9 during fatigue testing. The Gaussian envelope of the sinusoidal input is no longer distinguishable in the time series data. From the spectrogram, Figure 5(F), the active vibration input can be distinguished from the operational noise, which is most significant below 1,000 Hz.

Time series signals from all accelerometers are plotted in Figure 6 for excitation frequencies $f = [750\ 1,000\ 1,250\ 1,500\ 2,000]$ Hz. Depending on the sensor placement, the vibration amplitude at the excited frequencies can be observed to vary. Furthermore, for some of the sensor locations, the envelope of the vibration signals differs from the Gaussian envelope of the input excitation; the time stamps associated with the maximum vibration amplitudes differ across frequencies for some sensors; and the vibration signals continue after the cutoff of excitation at 3 seconds for some frequencies. Considering the noise floor, Figure 7 shows the power spectral density estimate of the actuator response during stand-still as well as the noise floor during stand-still and fatigue testing, respectively. The amplitude of ambient noise present during fatigue testing is significantly higher than during stand-still, being of highest amplitude below 600 Hz. Thus, for all frequencies used for the applied sinusoidal signal, the signal-to-noise ratio is high for both operational states, with a minimum signal-to-noise ratio for all signals and sensors of approximately 30 dB at $f = 1,000$ Hz for sensor 7.

2.4 | Data pre-processing

Based on the sensor data recorded during blade testing, the following pre-processing steps were applied before feature extraction:

- Mean removal
- Bandpass filtering with a digital filter to reduce ambient noise and noise from the fatigue exciter, using bandpass frequencies of ±50 Hz of the applied active vibration input frequency, with upper and lower stopband frequencies at 25 Hz below and above the lower and upper bandpass frequencies, respectively, with a stopband attenuation of 60 dB
- Trimming of data by removing the first second of data, where no excitation was applied
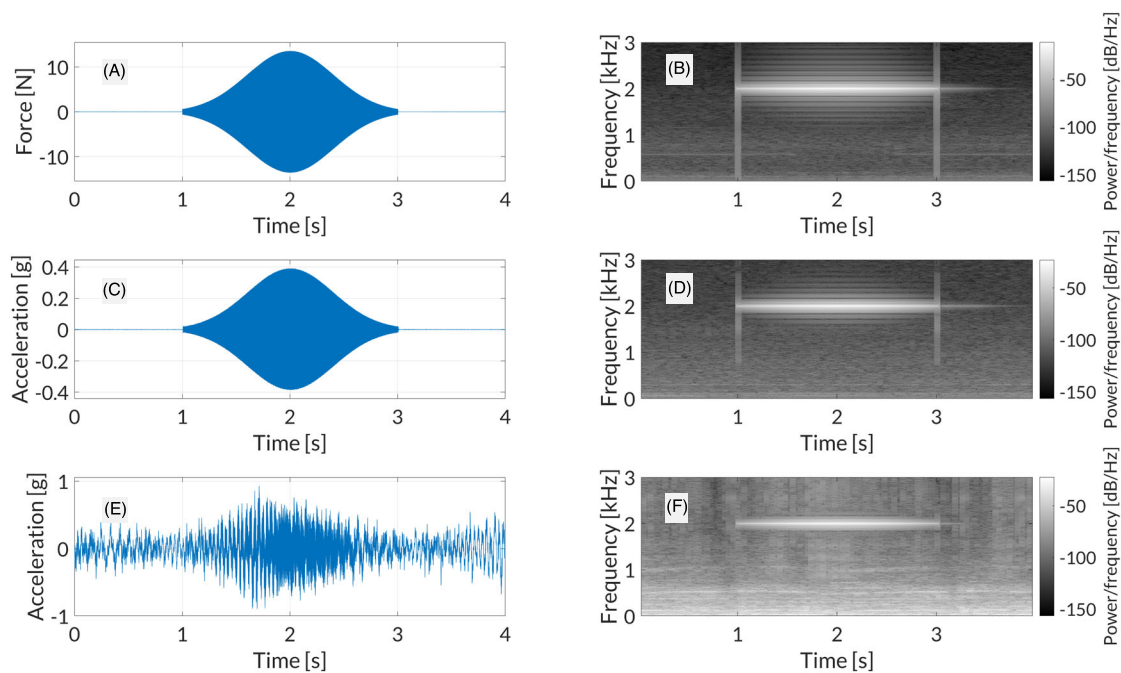
FIGURE 5 Sinusoidal signal at 2,000 Hz with Gaussian envelope. Force input time series (A), frequency response of force input (B), time series of acceleration response measured with accelerometer 9 during stand-still (C) and associated frequency response (D), as well as time series of acceleration response measured with accelerometer 9 during fatigue testing (E) and associated frequency response (F).
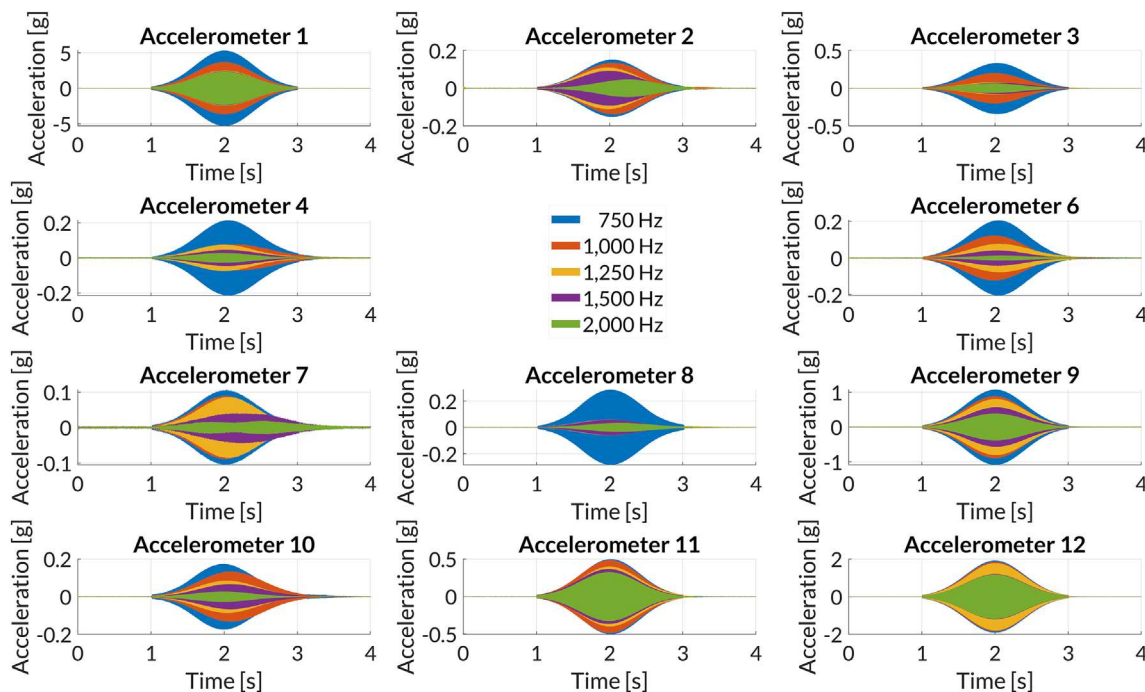
FIGURE 6 Acceleration data recorded during stand-still, given input signals at $f = [750\ 1,000\ 1,250\ 1,500\ 2,000]$ Hz with Gaussian envelope.

As shown previously, data recorded during fatigue testing is subject to much operational noise. To reduce some of this noise, filters have been applied to the time series data. Due to the application of sinusoidal signals with single frequencies, a relatively narrow bandpass filter can be applied. As shown previously in Figure 7, the signal-to-noise ratio is high in the frequency range between 750 and 2,000 Hz, where sinusoidal signals were applied. Thus, much of the noise in the time series signal, primarily present in frequencies below 600 Hz, can be removed by application

of a bandpass filter. The difference between the raw and bandpass filtered time series data is shown in Figure 8, where the Gaussian envelope of the vibration amplitude is clearly distinguishable in the filtered data (Figure 8(B)).

To reduce the length of the signal, the first second of the signal was trimmed, since no excitation was applied during this period. The last second of the signal, where no active excitation was applied either, was retained since it was found that some frequency content from the active input was still present, as shown in Figure 6, most likely stemming from reflections of the original input signal. It was chosen to retain this part of the signal, since it could potentially include damage-sensitive features.

2.5 | Signal processing for feature extraction

In the present work, signal processing methods used for feature extraction are based on quantifying the amplitude distribution of the applied sinusoidal signal. For this purpose, statistical measures are used as features. Additionally, the time series data is approximated through a linear regression model, and the model parameters are used as features for damage detection. Lastly, the time-frequency response at the given input frequencies is extracted.

2.5.1 | Statistical measures

To characterize a distribution, such as the amplitude distribution of the output signals resulting from the sinusoidal input signal, statistical moments are commonly applied. In this case, the statistical moments used are the root mean square (RMS) x_{RMS}, standard deviation σ, skewness s, and kurtosis k.[44–46] Additional statistical measures have been applied to establish an approach for SHM using dynamic measurements,[47] based on which the peak value x_{peak} and associated time stamp t_{peak} are also selected to be used, as presented in the following. The statistical measures used in this work are shown in Table 1.

The feature x_{peak}, being the peak value of an observation $\mathbf{x}$, accounts for the possibility of a negative value having the largest magnitude by taking the maximum absolute value from the observation. Due to noise being present in the signal, the average of the ten peak values from a single observation is used. The time stamp associated with the peak value, denominated t_{peak}, is used as a feature to characterize the distribution of
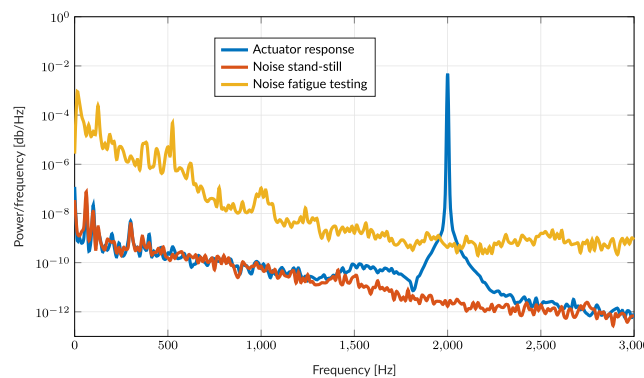

FIGURE 7 Frequency response of acceleration measurements, showing the amplitude of the sinusoidal signal, at 2,000 Hz in this case, as well as the noise floor during stand-still and fatigue testing, respectively. Measurements from accelerometer 9 were used, see Figure 4.
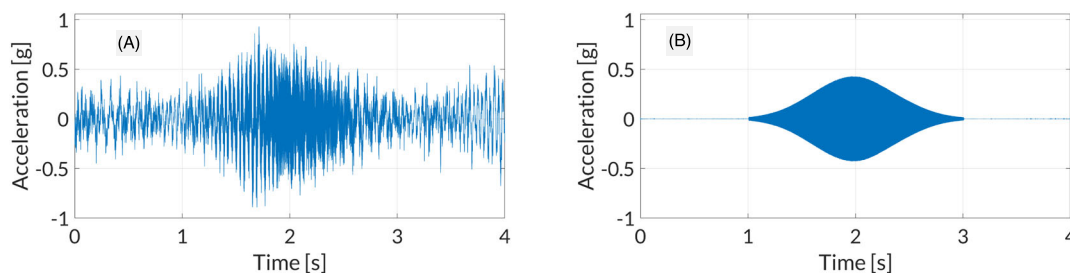

FIGURE 8 Acceleration time series (A) and same signal with bandpass filter applied (B).

TABLE 1 Statistical measures used for feature extraction.

$x_{peak} = \max\left(\left\|\{x\}_{n=1}^{N}\right\|\right)$	$t_{peak} = t(x_{peak})$
$x_{RMS} = \sqrt{\frac{1}{N}\sum_{n=1}^{N} x_n^2}$	$\sigma = \sqrt{\frac{1}{N-1}\sum_{n=1}^{N} \|x_n - \mu\|^2}$
$s = \dfrac{\frac{1}{N}\sum_{n=1}^{N}(x_n-\mu)^3}{\left(\sqrt{\frac{1}{N}\sum_{n=1}^{N}(x_n-\mu)^2}\right)^3}$	$k = \dfrac{\frac{1}{N}\sum_{n=1}^{N}(x_n-\mu)^4}{\left(\frac{1}{N}\sum_{n=1}^{N}(x_n-\mu)^2\right)^2}$

N: Number of observations.   Mean: $\mu = \frac{1}{N}\sum_{n=1}^{N} x_n$

the vibration output. Figure 9(A) illustrates the time series response from one of the accelerometers, recorded in the healthy and damaged state of the blade, respectively. The peaks of the two observations, denominated $x_{peak,h}$ and $x_{peak,d}$ for the healthy and damaged state, respectively, as well as the associated time stamps are marked in the figure. A change in both the peak value of the amplitude and the time stamp associated with the peak value can be observed.

Due to the applied sinusoidal signals being oscillating, the use of the mean is not necessarily an appropriate measure for the signal, since positive and negative values will cancel out. Thus, the RMS is used as a feature in this work. The standard deviation σ is a measure of the variation of a distribution with respect to its mean value. Together with the mean μ, the standard deviation is used to define a normal distribution $\mathcal{N}(\mu,\sigma)$, such as the one used for the sinusoidal signals with Gaussian envelope applied with the vibration shaker. The skewness s characterizes the asymmetry of a distribution around the sample mean. A normal distribution, which is symmetric, has a skewness equal to zero. The kurtosis k is a measure of the proneness of a distribution to outliers.

The listed statistical measures are used to characterize output measurements, given the application of active vibration excitation with a Gaussian envelope. The statistical measures are applicable for extraction of features from time series or frequency domain data, yielding a total of six scalar features, regardless of the dimensionality of the original data.

2.5.2 | Auto-regression

Auto-regressive (AR) models are used in linear prediction of discrete signals, i.e. fitting a model to data of the past behavior of a system. Based on the past behavior of the system, the model may be used to predict the future behavior of the system.[48] Considering the known measurements of a discrete-time signal $x(n)$, with n assuming an integer value, an AR model of $x(n)$ can be expressed in the form[48,49]:

$$x(n) + \sum_{i=1}^{p} a(i)x(n-i) = e(n) \tag{1}$$

where p is AR model order, $\{a(i)\}_{i=1}^{p}$ are the so-called AR parameters, $\{x(n-i)\}_{i=1}^{p}$ are the p past measurements of the known measurements used to predict the future behavior of a system, and $e(n)$ is the prediction error. The AR parameters $\{a(i)\}_{i=1}^{p}$ can in practice be determined by minimizing the prediction error $e(n)$ in Equation (1) with respect to the AR parameters. In this work, the AR models fitted to the available time series data are not used to predict the future behavior of the system, but instead, the AR parameters are used as features for damage detection.

2.5.3 | Hilbert transform

The Hilbert transform of a signal $x(t)$ yields the so-called analytic signal $z(t)$:

$$z(t) = x_r(t) + jx_i(t) \tag{2}$$

with a real part $x_r(t)$, corresponding to the original signal, and an imaginary part $x_i(t)$, which is the Hilbert transform of the original signal. The Hilbert transform is a version of the original signal with a 90° phase shift, having the same amplitude and frequency content as the original signal. One of the properties of the Hilbert transform is that its magnitude corresponds to the envelope of the original signal.[50] This property is utilized in the present work to extract the amplitude distribution of the vibration output, which is used as a feature for detection of damage in the blade. This is done through use of the previously presented statistical measures. The Hilbert envelope of the time series data plotted in Figure 9(A) is shown in Figure 9(B).
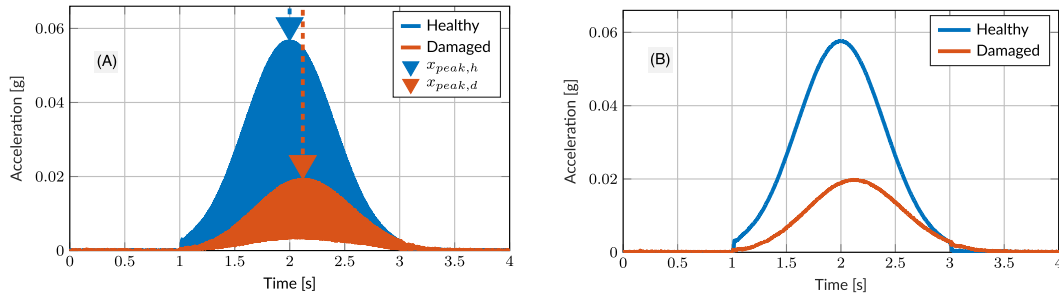
FIGURE 9 (A): Absolute values of time series output from accelerometer 8, sampled in the healthy and damaged state during stand-still with bandpass filter applied. An active vibration input at $f = 2,000$ Hz was applied. (B) Hilbert envelope of time series data in (A).

2.5.4 | Short-time Fourier transform

The short-time Fourier transform (STFT) is used to analyze time-frequency behavior of non-stationary signals. The STFT is calculated by sliding a window $w(n)$ with length M over the time series signal and calculating the discrete Fourier transform (DFT) for each windowed segment of data[51]:

$$X_m(f) = \sum_{n=0}^{N-1} x(n)w(n-mR)e^{-j2\pi fn}; \, m = 1,...,k \quad (3)$$

where $X_m(f)$ is the mth DFT, $R = M - L$ is the window hop size, L is the overlap between adjacent data segments, and mR is the time around which the mth window is centered. The number of data segments into which the original data is split is given as:

$$k = \left\lfloor \frac{N-L}{M-L} \right\rfloor \quad (4)$$

where the brackets $\lfloor \rfloor$ denote the floor function. The DFTs are then assembled into a matrix with k columns, the STFT, containing the time-frequency response of the original data. The length of the DFTs, and as such the number of rows in the STFT matrix, corresponds to the number of DFT points used. The STFT is commonly visualized through the spectrogram, see Figure 10(A), which is the magnitude squared of the STFT, showing the time-frequency behavior of a signal.

Following the calculation of the STFT, the column, i.e. frequency line, corresponding to the frequency of the sinusoidal input signal is extracted. The extracted data contains the amplitude distribution at the frequency of the sinusoidal input signal, in which changes are desired to be tracked and used to detect damage in the wind turbine blade. With the chosen window length, overlap, and DFT settings, this results in 420 DFT points per frequency line as features. The frequency line at the input frequency of $f = 2,000$ Hz, extracted from the STFT plotted via the spectrogram in Figure 10(A), is shown in Figure 10(B), including the same frequency line associated with time series data recorded in the damaged state of the blade.

For processing of the available data, one of the advantages of the STFT is the extraction of a single frequency line, making the method more robust to operational noise at frequencies other than the extracted frequency. Thus, bandpass filtering is not necessary to apply. The extracted amplitude distribution contains less operational noise in general, compared to e.g., the amplitude distribution extracted through use of the Hilbert transform. This is due to operational noise at frequency components other than that contained in the single extracted STFT frequency line being contained in the Hilbert envelope.

2.6 | Dimensionality reduction

To reduce the feature space, both for increased computational efficiency, as well as for increased performance in outlier detection, dimensionality reduction is performed. By reducing the dimensionality of the feature space to a point where only the damage-sensitive features are retained, thus discarding features that do not change significantly with introduction and propagation of damage, performance in outlier detection is increased. For this purpose principal component analysis (PCA) is used, which is a popular method for dimensionality reduction.[44] In PCA, the original data X is projected onto a space with lower dimensionality, with the choice of dimensionality of the projected space being dependent on the percentage of variance of the original data desired to be retained:
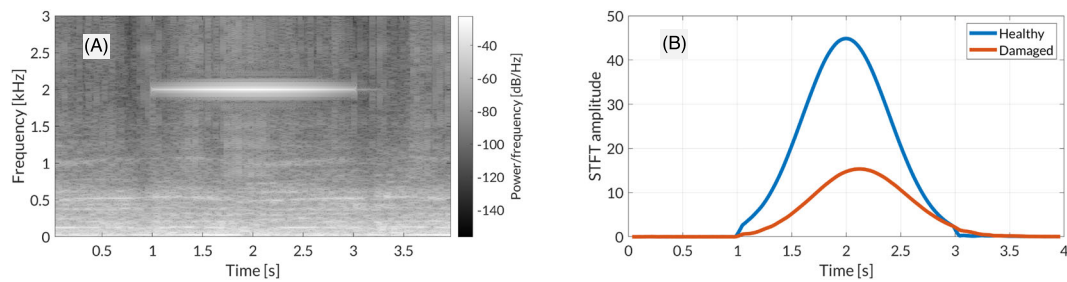
$$W = XV \quad (5)$$

FIGURE 10   Spectrogram of healthy time series data, extracted during fatigue testing with no bandpass filter applied; see Figure 8(A). (A) Single frequency line from STFT (B), extracted at $f = 2,000$ Hz.

where W is the projected data and V contains the principal component (PC) directions. The PCs are commonly calculated in descending order regarding the percentage of variance explained. Thus, the first PC will contain most information relating to the original data, followed by the second PC, etc. The number of PCs is commonly chosen based on retaining e.g., 95 or 99% of the variance of the original data. This choice also depends on how much noise is inherent in the original data, since a higher percentage of variance explained may also result in more random noise being retained in the projected data.

2.7 | Outlier analysis

To classify the health state of the tested wind turbine blade, outlier analysis is performed, using the Mahalanobis distance as an outlier detector. The Mahalanobis distance, which is a multivariate generalization of the Euclidean norm, is a commonly used distance metric in SHM.[27] Since the focus of the present work is on an engineering-based application of a monitoring system, and not the development of new algorithms for outlier analysis, a classical distance metric for outlier analysis is utilized. The Mahalanobis distance is a simple and well-known measure with good computational efficiency, and as will be presented in Section 3.2, high classification accuracy can be obtained by use of such a basic distance metric. The Mahalanobis distance is given as:

$$D_i = \sqrt{(y_i - \overline{X})^T S^{-1} (y_i - \overline{X})} \tag{6}$$

where y_i is the ith observation of the testing data set Y, in which potential outliers are desired to be discovered; $\overline{X}$ is the mean of the training data set X; and S is the covariance of the training data set X. Using the damage indices from the training data set X, a threshold value D_0 for the healthy state is determined. Any observations in the testing data set Y with a damage index exceeding the healthy threshold D_0 are consequently labeled as being in a damaged state. The threshold D_0 used in this work is based on a number of random trials, calculated from the mean and covariance of the training data set.[27] The threshold value D_0 is selected based on the $(100 - F)$th percentile of the random trials, corresponding to $F\%$ false positives.

3 | RESULTS

The following presents the features extracted using the presented signal processing methods, investigating damage sensitivity of the features; as well as results from outlier analysis, using the different features for detection of initiation and propagation of the shear web damage.

3.1 | Damage sensitivity of extracted features

The extracted features are examined in the following, investigating their damage sensitivity and its dependence on sensor placement and frequency of the applied sinusoidal vibration signals.

3.1.1 | Time series data: Statistical measures

Based on the active vibration signals recorded during the blade test, features are extracted for each observation. To visualize changes in the features caused by damage, features extracted from healthy observations are colored green, and features extracted from the initiation of the damage

until the end of the blade test are colored on a scale from yellow to red. Based on the time series data from accelerometer 9, see Figure 4, for input frequencies $f = [750 \; 1,000 \; 1,250 \; 2,000]$ Hz, features in the form of the statistical measures described in Section 2.5.1 are calculated and plotted in Figure 11. Each feature has its mean removed and is normalized with respect to the largest absolute value of the respective feature, resulting in equal scaling of the features. Based on data from a sinusoidal signal with frequency $f = 750$ Hz, the statistical measures x_{peak}, x_{RMS}, and σ exhibit a clear jump between the healthy and damaged observations, illustrating the sensitivity of the features to the initiation of the damage. With increasing damage severity, these features can be observed to change monotonically, showing their sensitivity to damage progression. For the remaining statistical measures, t_{peak}, s, and k, the observations from healthy and damaged states show significant overlap and no clear distinction between healthy and damaged states.

For sinusoidal signals with frequencies $f = [1,000 \; 1,250]$ Hz applied, there is no clear separation between features in healthy and damaged states. Generally, the overlap is lower for the features x_{peak}, x_{RMS}, and σ compared to t_{peak}, s, and k. For $f = 1,000$ Hz, observations from the damaged state show no clear progression in line with increasing damage severity, i.e. damage progression cannot be inferred directly from the features extracted at $f = 1,000$ using accelerometer 9. With $f = 1,250$ damage progression can be inferred to some degree, but the overlap between observations at different degrees of damage severity is still high.

With applied sinusoidal signals of frequency $f = 2,000$, observations of the features are similar to those for $f = 1,000$ Hz. One major difference is the features x_{peak}, x_{RMS}, and σ becoming more similar in value to the healthy state with increasing damage severity. Consequently, the healthy and damaged states should be separable, but tracking of increasing damage severity may not be monotonic.

Considering the features extracted from accelerometer 7, see Figure 12, which is the sensor placed farthest from the shear web damage, the features generally overlap in the healthy and damaged states. For a sinusoidal signal with frequency $f = 1,000$ Hz applied, the features t_{peak}, s, and k show less variation in the damaged state than in the healthy state. With a sinusoidal signal at frequency $f = 2,000$ Hz, x_{peak}, x_{RMS}, and σ exhibit monotonic change in the feature values in line with damage progression, but with no clear separation between the healthy state and the damaged state with lowest damage severity.

3.1.2 | Auto-regressive parameters

The model order of the AR model is chosen as $p = 40$, based on an investigation of the modeling accuracy of the original signal and the Bayesian information criterion,[49] which penalizes for model complexity, reducing the likelihood of model overfitting. This model order fits well for all sensor
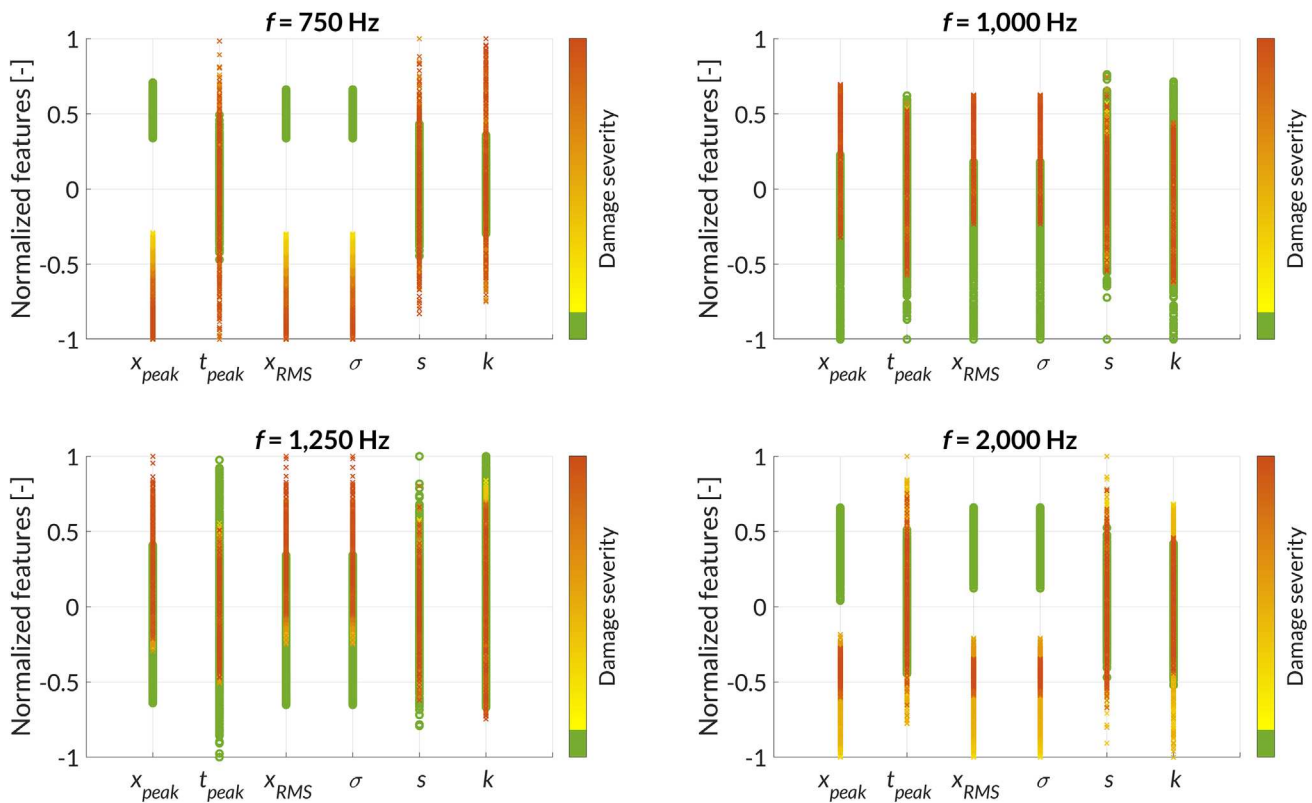

FIGURE 11 Statistical measures extracted from time series data from accelerometer 9, placed on the shear web laminate.
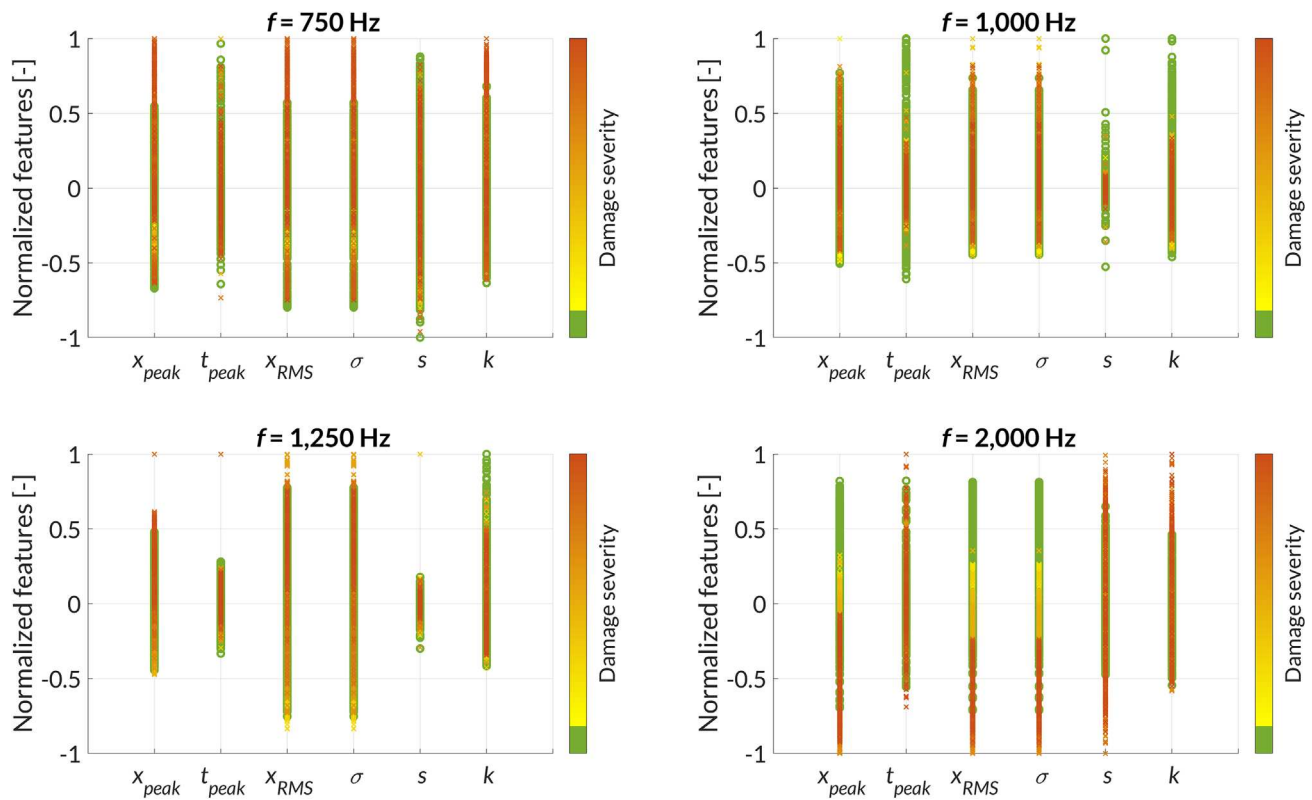
FIGURE 12 Statistical measures extracted from time series data from accelerometer 7, placed on the shell laminate.

channels, and the same model order is thus used for every channel. A more thorough investigation regarding the influence of the AR model order on classification accuracy may be found in, for example, Panagiotopoulos et al.[42] Using the AR model order $p = 40$, the AR parameters $\{a(i)\}_{i=1}^{p}$ are calculated for all available observations of the bandpass filtered accelerometer data. The extracted AR parameters are plotted in Figure 13. In general, some distinction between the healthy and damaged states can be observed in the AR parameters, but no clear separation is present between healthy and damaged states. Due to the high dimensionality of the data, this separation may, however, still be obtained when performing outlier analysis. For some of the AR parameters, two major clusters seem to be present for observations in the healthy state, see e.g., the tenth AR parameter for frequencies $f = [750 \ 1,000]$ Hz, which is most likely due to differences present in the signal during stand-still and fatigue testing. Thus, some of the AR parameters may be useful for distinguishing between the operational states of the blade.

3.1.3 | Hilbert envelope: Statistical measures

For each observation of the available accelerometer data, the absolute value of the Hilbert transform is calculated, yielding the envelope of the time series data. Having applied bandpass filtering to the time series data, the amplitude distribution of the Hilbert envelope corresponds accurately to the Gaussian envelope of the vibration output. Based on the Hilbert envelope, the statistical measures outlined in Section 2.5.1 are calculated and used as features. The features extracted through the presented approach are plotted in Figure 14, based on data from accelerometer 9 and input frequencies $f = [750 \ 1,000 \ 1,250 \ 2,000]$ Hz applied by the vibration shaker. Similar to the observations presented for the statistical measures extracted from the time series data, with a sinusoidal signal with frequency $f = 750$ Hz the features x_{peak}, x_{RMS}, and σ exhibit a clear separation between healthy and damaged observations, including monotonic progression in line with the increase in damage severity. The remaining features display a high degree of overlap between healthy and damaged states, however to a lower degree than the statistical measures extracted from the time series data. In general, the distribution of the features is very similar to that observed for the features extracted from the time series data.

3.1.4 | Short-time Fourier transform

Differing from the previous feature extraction methods, no bandpass filter is applied for the STFT. Since a single frequency line, at the frequency of the active vibration input, is extracted, bandpass filtering does not affect the extracted frequency response. For calculation of the STFT, a
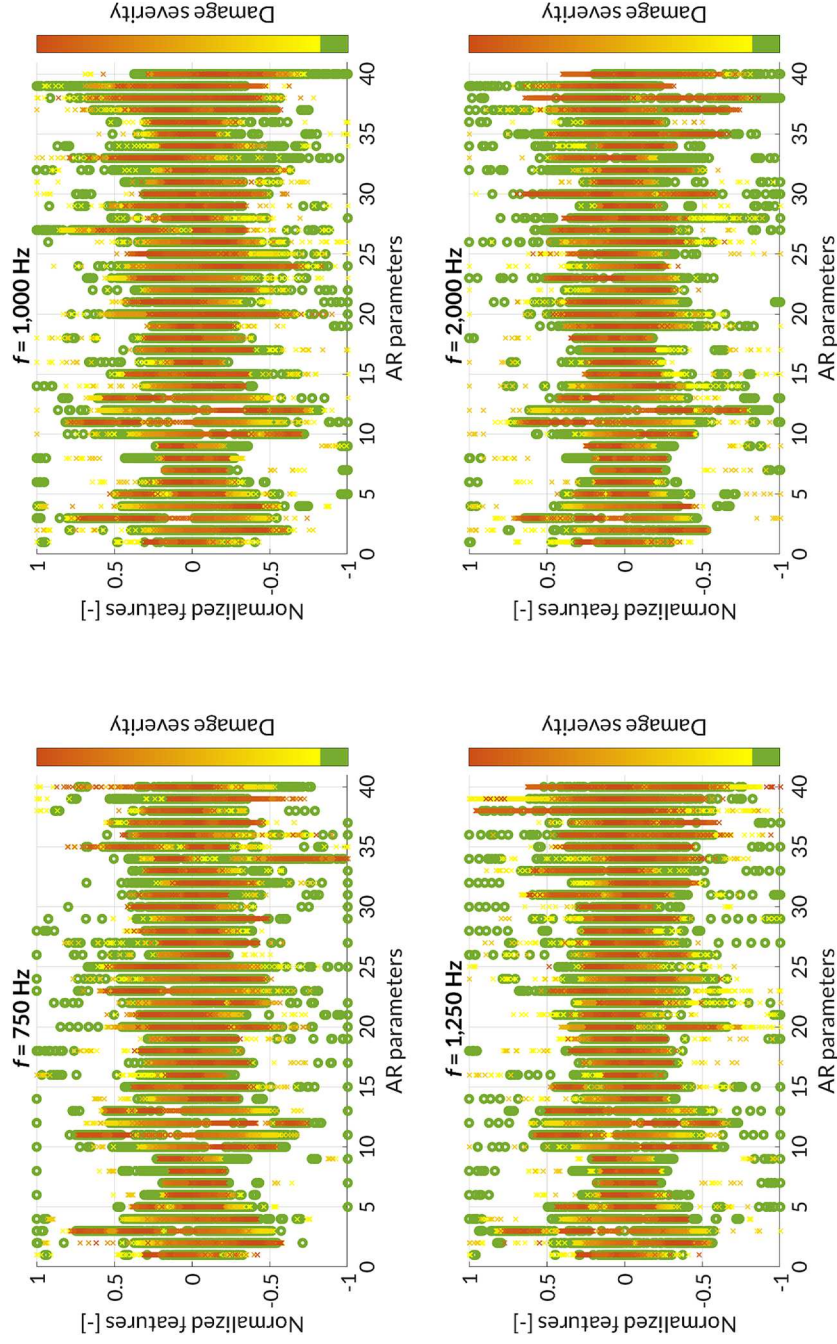
FIGURE 13 AR parameters extracted from time series data from accelerometer 9, placed on the shear web laminate.
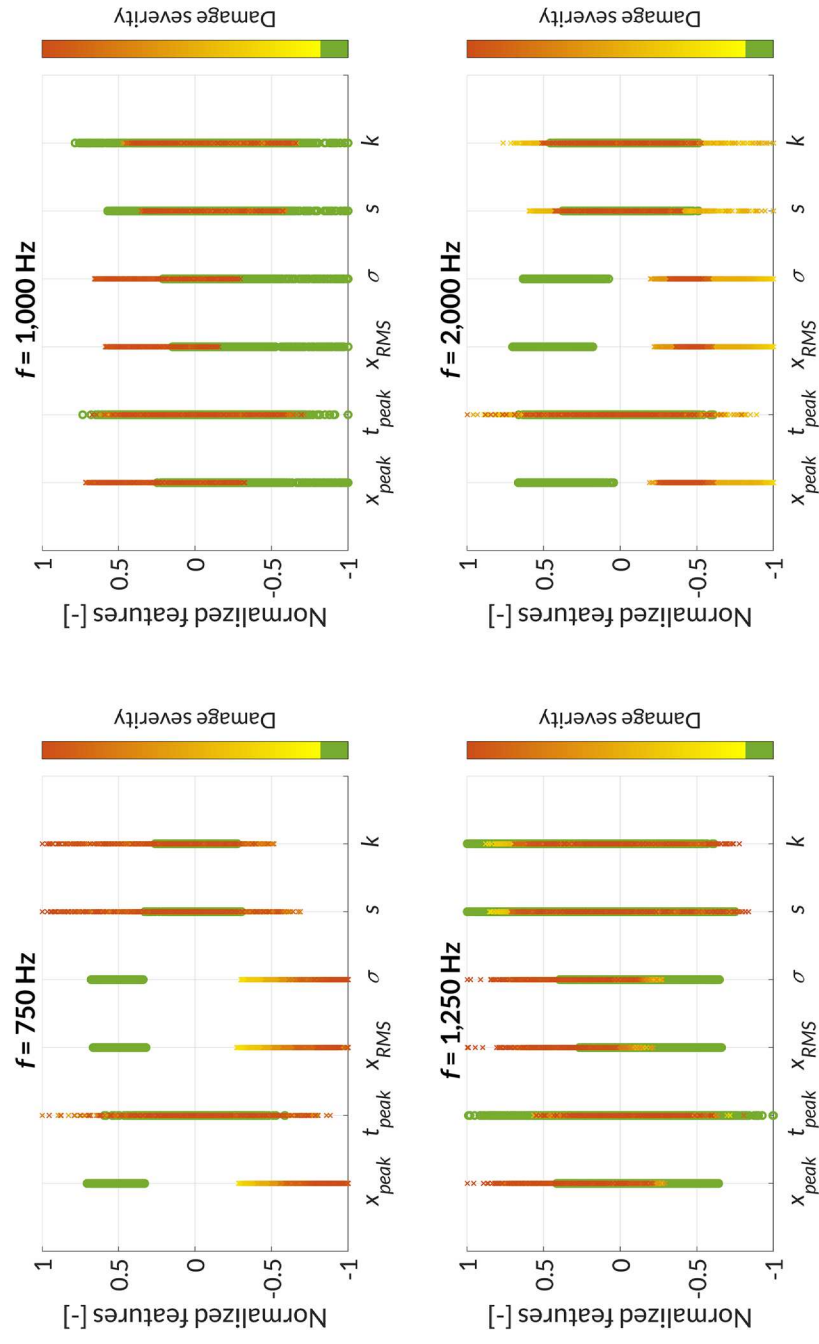

FIGURE 14 Statistical measures extracted from Hilbert envelope of time series data from accelerometer 9, placed on the shear web laminate.

Tukey window is used, which is equal to unity for a majority of the window length, yielding a narrow main lobe and thus good separation of frequency components, at the cost of lower side lobe attenuation. Since a single frequency line at the frequency of the active vibration input is extracted, high side-lobe attenuation is not required. An overlap L of adjacent data segments corresponding to 90% of the window length M is used, resulting in smoothing of some of the noise inherent in the signals.

Based on the available time series data, the STFT is calculated, and the frequency lines corresponding to the frequencies of the applied sinusoidal signals are extracted, as plotted in Figure 15 for accelerometer 9. Generally, the observations made for the STFT frequency lines correspond well to the previous observations made for the statistical measures calculated based on the time series data and the Hilbert envelope. For the STFT frequency line extracted at 750 Hz, a clear jump between the frequency amplitude in the healthy and damaged state can be observed, followed by monotonic decrease in the amplitude with increasing damage severity.

3.2 | Outlier detection

In the following, the previously presented features, extracted from data relating to excitation frequencies $f = [750 \ 1,000 \ 1,250 \ 2,000]$ Hz, are used to perform outlier detection, comparing the performance in classification accuracy by use of the different features. The used data includes observations sampled during stand-still and fatigue testing for both the healthy and damaged state. Dimensionality reduction using PCA is performed for all features, using PCs explaining 99.99% of the variance of the original data for the statistical measures, 99% for the AR parameters, and 97% for the STFT frequency lines. To calculate the healthy threshold D_0, every second observation of the first 90% of the healthy observations is used. The healthy training data set is chosen in this manner to account for variations in operating conditions, caused by fluctuations in the load applied by the rotating mass fatigue exciter.

Damage indices, calculated using Equation (6), using data from accelerometer 7 are plotted in Figure 16, using the same features as previously described. For this sensor location, using the statistical measures calculated based on time series data and the Hilbert envelope, respectively, performance is poor in classifying the damaged state of the blade. Only a minor percentage of the damaged observations, primarily toward the most significant damage severity, are above the healthy threshold value. This is deemed to be due to changes in the feature space resulting from the operational state being more significant than changes resulting from damage initiation and progression. Thus, when performing dimensionality
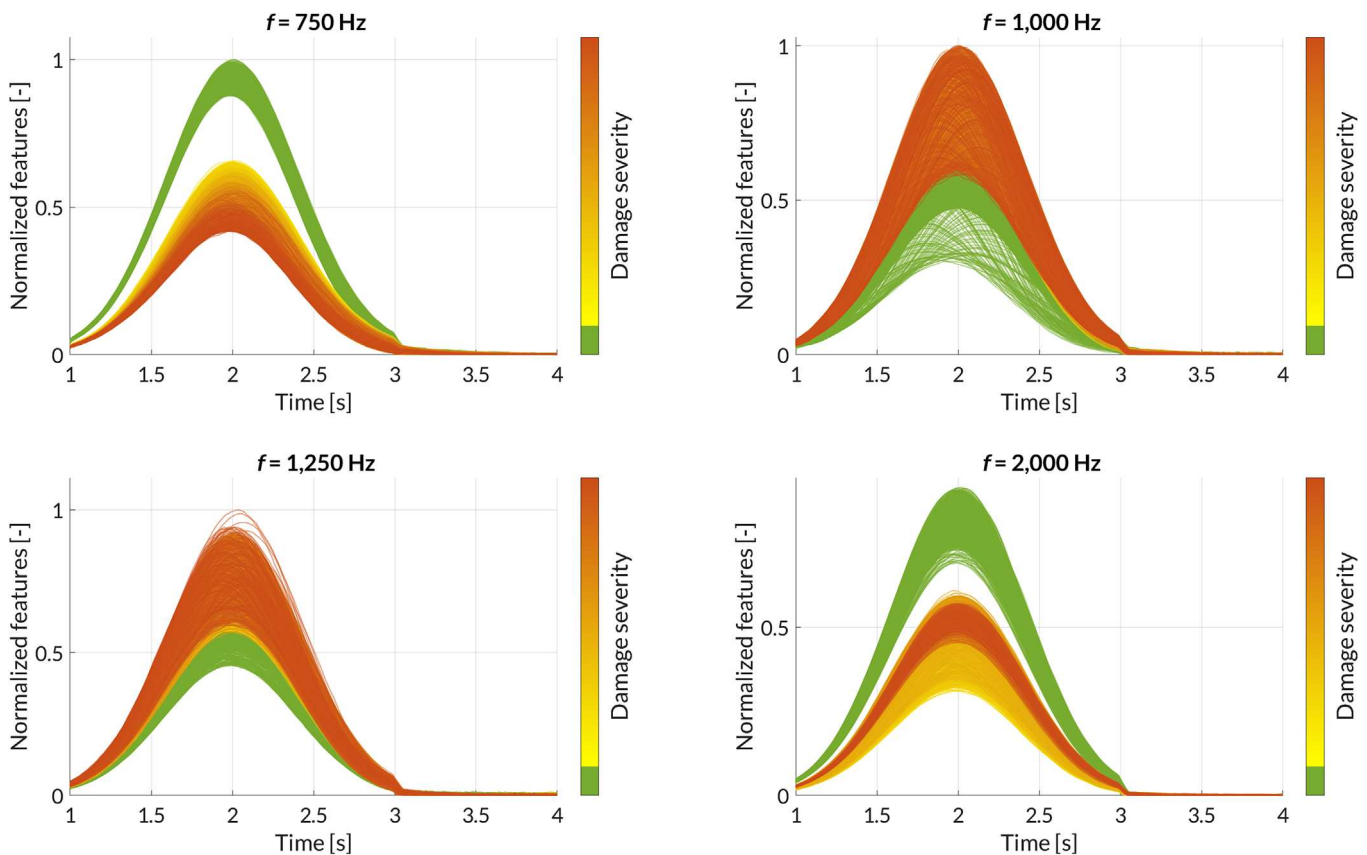

FIGURE 15 STFT frequency lines at $f = [750 \ 1,000 \ 1,250 \ 2,000]$ Hz, respectively, from accelerometer 9.
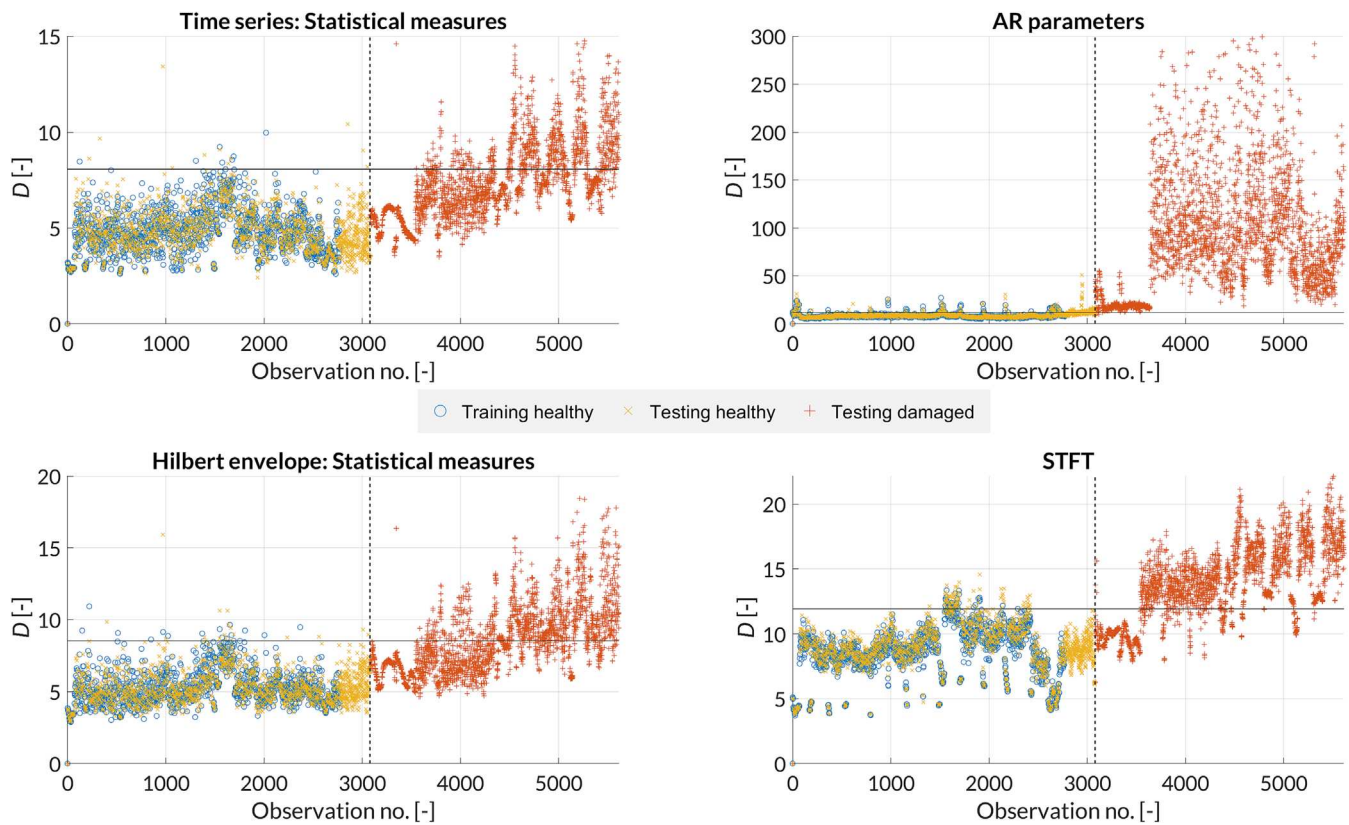
FIGURE 16 Damage indices D calculated using the four different presented features, based on accelerometer signals recorded with accelerometer 7 during active vibration excitation at frequencies $f = [750\ 1,000\ 1,250\ 1,000\ 2,000]$ Hz. Threshold D_0 is indicated through horizontal lines; point of manual damage introduction is marked with vertical dotted lines.

reduction with PCA, features including changes in the operational state are weighted higher than damage-sensitive features, which results in poor separation between observations in the healthy and damaged states. The operational state is observed to have increasing influence with increasing distance from the used accelerometer and the vibration shaker. The influence of the operational state on damage sensitivity of the features will be investigated further in the following. Using AR parameters as features, classification accuracy is higher for sensor 7 than for the previously shown results from sensor 9, even though the present sensor is located further away from the damage and on another part of the blade structure. The observations recorded in the damaged state with damage indices below the healthy threshold were all recorded during stand-still. Thus, the features based on AR parameters are missing information, which can separate the damaged observations during stand-still from the healthy observations during both stand-still and fatigue testing. For the STFT, performance is good for this sensor location, with most of the damaged observations being classified above the healthy threshold, including progressive increase of the damage index in line with damage progression.

Instead of using PCA to automatically apply weights to features, features may be picked manually, based on existing knowledge regarding their damage sensitivity. Thus, obtained results in outlier analysis look very different, as shown in Figure 17. For this example, the feature x_{RMS} from vibration data at an active excitation frequency $f = 2,000$ Hz is used for the statistical measures of both the time series data and the Hilbert envelope, respectively. The feature x_{RMS} is chosen based on inspection of Figure 12, where gradual change of the feature in line with damage progression can be observed. For AR parameters and the STFT, the features extracted from $f = 2,000$ Hz are used to facilitate comparison, not performing PCA to reduce the feature space. Using features picked based on knowledge on damage sensitivity changes the classification accuracy significantly for some of the signal processing methods: Time series statistical measures 54.41% to 75.59%; AR parameters 96.58% to 95.51%; Hilbert envelope statistical measures 64.49% to 76.96%; and STFT frequency line 82.27% to 66.94%. Thus, the features based on statistical measures show greatly improved classification accuracy, with clear separation between part of the damaged observations and the healthy observations. This is much in line with the change of the features observed in Figure 12, where x_{RMS} partly overlaps between observations in the healthy and damaged states. For the AR parameters, performance is decreased slightly. However, the damage index exhibits a somewhat linearly increasing trend, being more in line with damage progression than what can be observed for the AR parameters in Figure 16. For the STFT frequency line, performance is significantly decreased through manual feature picking and omitting PCA. Classification accuracy of healthy testing observations is poor, with observations sampled during fatigue testing mostly being classified above the healthy threshold. In contrast, damaged observations sampled during stand-still are classified below the healthy threshold. Thus, the manually picked STFT feature enables separation between
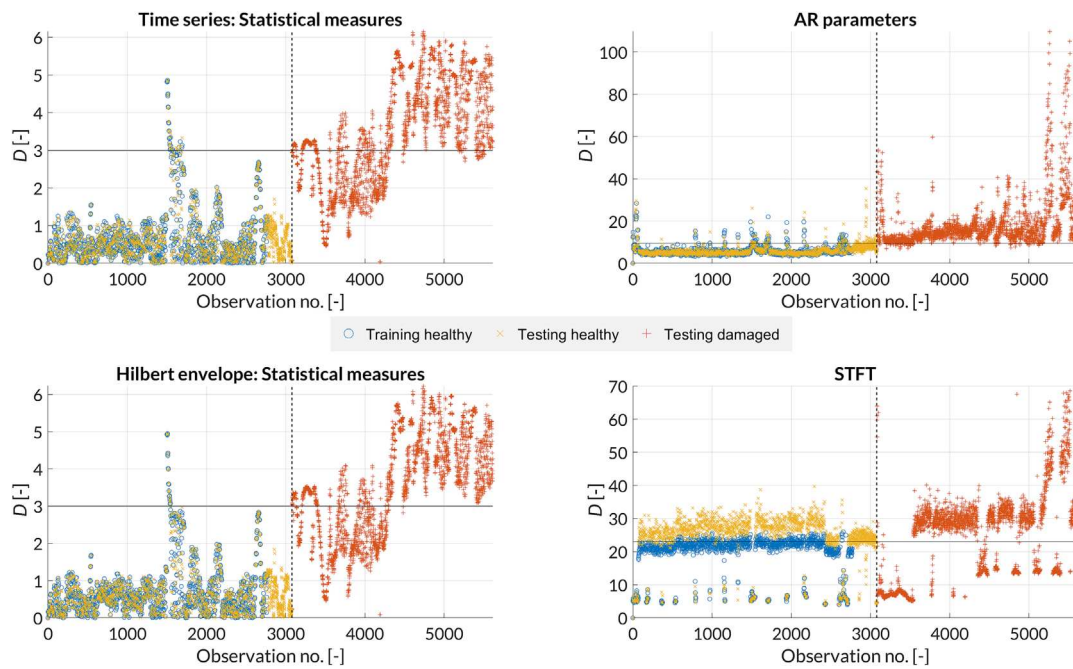
FIGURE 17 Damage indices D calculated using the four different presented features, based on accelerometer signals recorded with accelerometer 7 during active vibration excitation at frequencies $f = 2,000$ Hz. Features are picked manually, and PCA is not performed. Threshold D_0 is indicated through horizontal lines; point of manual damage introduction is marked with vertical dotted lines.

the operational states, but damage sensitivity is lost. As such, there are pros and cons for automated vs. manual feature picking for the different signal processing methods, which show to be very different across the investigated feature spaces.

Damage indices based on measurements from accelerometer 9 are plotted in Figure 18, using data from excitation frequencies $f =$ [750 1,000 1,250 1,000 2,000] Hz. The features based on calculation of statistical measures, both from the time series signal and from the Hilbert envelope, result in damage indices that exhibit a clear jump in magnitude after introduction of the damage, yielding clear separation between the healthy and damaged states. The damage indices calculated based on these features also exhibit a slight linearly increasing trend with increasing observation number for the latter half of the observations recorded in the damaged state of the blade. The damage indices calculated based on AR parameters also exhibit a clear separation between healthy and damaged states, with a decreasing linear trend with increasing damage severity. The damage indices calculated based on the STFT frequency lines extracted at the frequencies of the active vibration excitation show a clear separation between healthy and damaged states, but no significant increase in line with progression of the damage.

In the same manner as previously done for accelerometer 7, features are manually chosen for comparison for accelerometer 9, using features from excitation frequency $f = 750$ Hz, which based on inspection of x_{RMS} in Figure 11 can be observed to exhibit clear separation between healthy and damaged states as well as monotonic increase in line with damage severity. The feature x_{RMS} is used for the time series data and Hilbert envelope, respectively, and all AR parameters and DFT points based on the excitation frequency $f = 750$ are used as features. The resulting outlier plots are shown in Figure 19, where the use of the statistical measure x_{RMS} for the time series data and Hilbert envelope, respectively, yields clear trends of linear increase in line with damage progression. This is much improved compared to the trends exhibited for the features extracted from the statistical measures using PCA, as plotted in Figure 18. For the AR parameters, the damage indices also show an increasing trend, which follows the increasing damage severity over the course of the fatigue test, compared to the decreasing trend observed when using features picked through PCA. Additional variability can be observed after observation no. 5000, most likely due to some of the AR parameters being sensitive to operational variations. For the STFT frequency line, a major difference between using PCA to reduce the feature space and manually picking the STFT frequency line from a damage-sensitive frequency is the separation of observations sampled in the operational states of stand-still and fatigue testing. Observations sampled during stand-still have a much lower damage index than observations sampled during fatigue testing, being approximately between 0-10 and 20-40, respectively, in the healthy state. The healthy testing observations sampled during fatigue testing are mostly classified above the healthy threshold. The damaged observations sampled immediately following the manual introduction of the damage are sampled during stand-still, and can be seen to be mostly classified below the healthy threshold. However, the damage indices for these observations are significantly higher than those for the healthy observations sampled during stand-still. Generally, the observations in the damaged state exhibit an increasing trend in line with damage progression.

The classification accuracy, calculated as the percentage of correct classifications of the healthy testing and damaged testing data, is shown for the different feature extraction methods applied to every accelerometer channel in Table 2. Performance for all features is high for the sensors
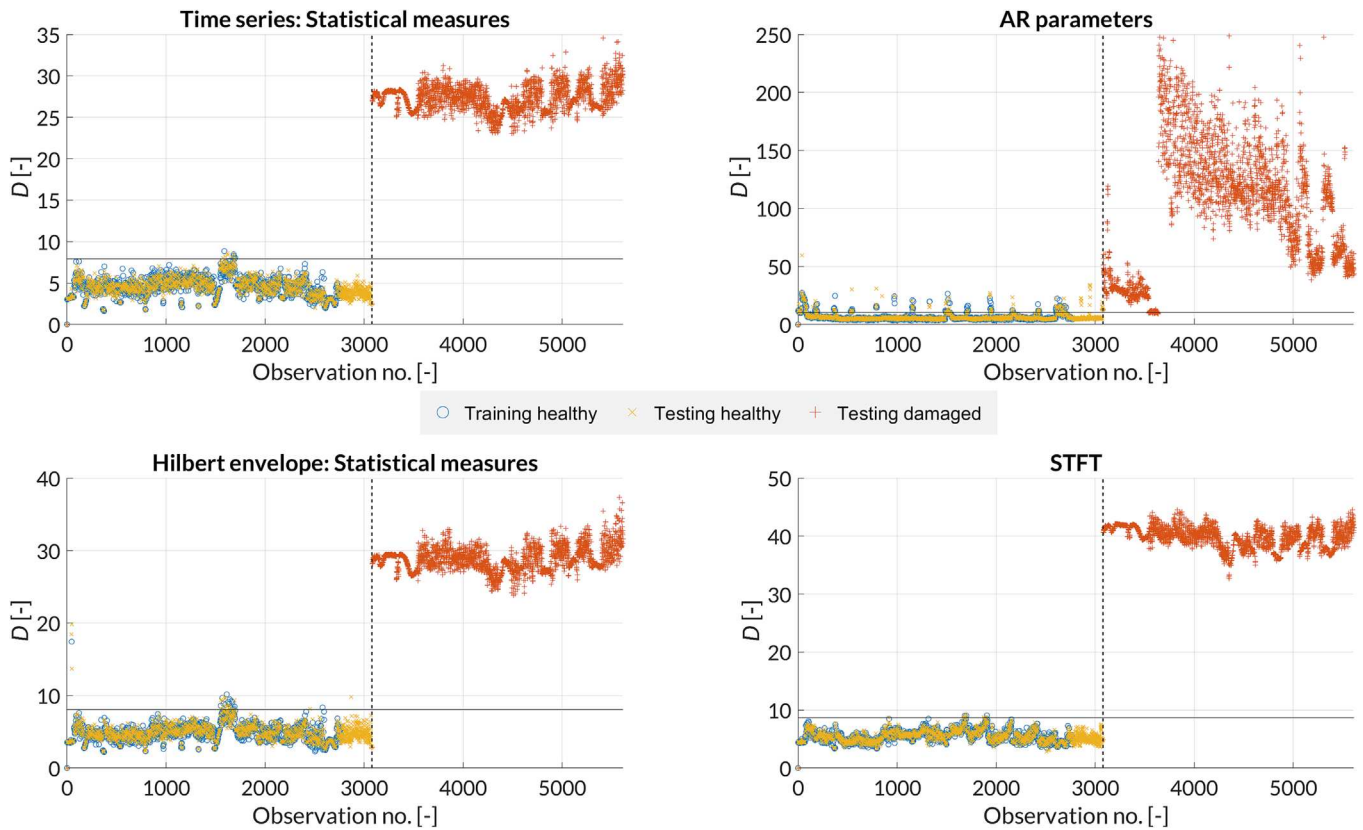
FIGURE 18 Damage indices D calculated using the four different presented features, based on accelerometer signals recorded with accelerometer 9 during active vibration excitation at frequencies $f = [750\ 1,000\ 1,250\ 1,000\ 2,000]$ Hz.

placed on the shear web. The statistical measures extracted from the time series data generally yield the lowest performance for sensors placed on the shell and spar cap laminate, with the statistical parameters extracted from the Hilbert transform yielding higher performance for these sensors. For the features based on statistical measures, classification accuracy is generally observed to decrease with increasing distance of the sensors to the vibration input. Using the STFT frequency lines yields reasonably good performance for all sensors, i.e. above 82%, while the AR parameters result in the best overall performance with a minimum classification accuracy of 92%. Thus, AR parameters provide damage-sensitive features, which are robust to changes in the operational condition, given the time series data being filtered as previously described. Not filtering the time series data would yield results similar to those for the STFT shown in Figure 17. The sensor for which performance is lowest varies across the different features: sensor 2 for the statistical measures, sensor 6 for the AR parameters, and sensor 7 for the STFT frequency lines. Common for all these sensors is their placement on the shell laminate, requiring the vibration signals to travel through various geometry transitions, which are deemed to have a significant effect on decreasing the vibration amplitudes.

4 | DISCUSSIONS

With the applied sinusoidal signals, a Gaussian envelope was applied to enable tracking of the amplitude distribution of the accelerometer outputs. It was observed that the features x_{peak}, x_{RMS}, and σ changed in similar manners, and the same is somewhat true for t_{peak}, s, and k. The first three features characterize changes in amplitude, while the last three features characterize changes in the amplitude distribution. Depending on the frequency of the active vibration input, sensor location, and damage type, either or both of these attributes may be damage-sensitive. Due to the similarity in the features x_{peak}, x_{RMS}, and σ, it is redundant to use all three, and the features space could thus be reduced to e.g., x_{RMS}. The features s and k show similar trends, but they are both deemed to be useful, while the feature t_{peak} may be discarded since it provides information similar to that contained in s and k.

Using the vibration shaker, sinusoidal signals between 750 and 2,000 Hz were applied. Inspection of the features extracted from the accelerometer measurements associated with the different applied frequencies showed that the damage-sensitive frequencies were dependent on sensor location. Generally, the chosen frequency range enabled good performance in detection of damage initiation and progression, at least for some of the chosen features. Thus, the chosen frequency range is deemed to be useful for blade SHM, providing a good trade-off between detectable damage size and detection range, while being somewhat insensitive to operational noise.
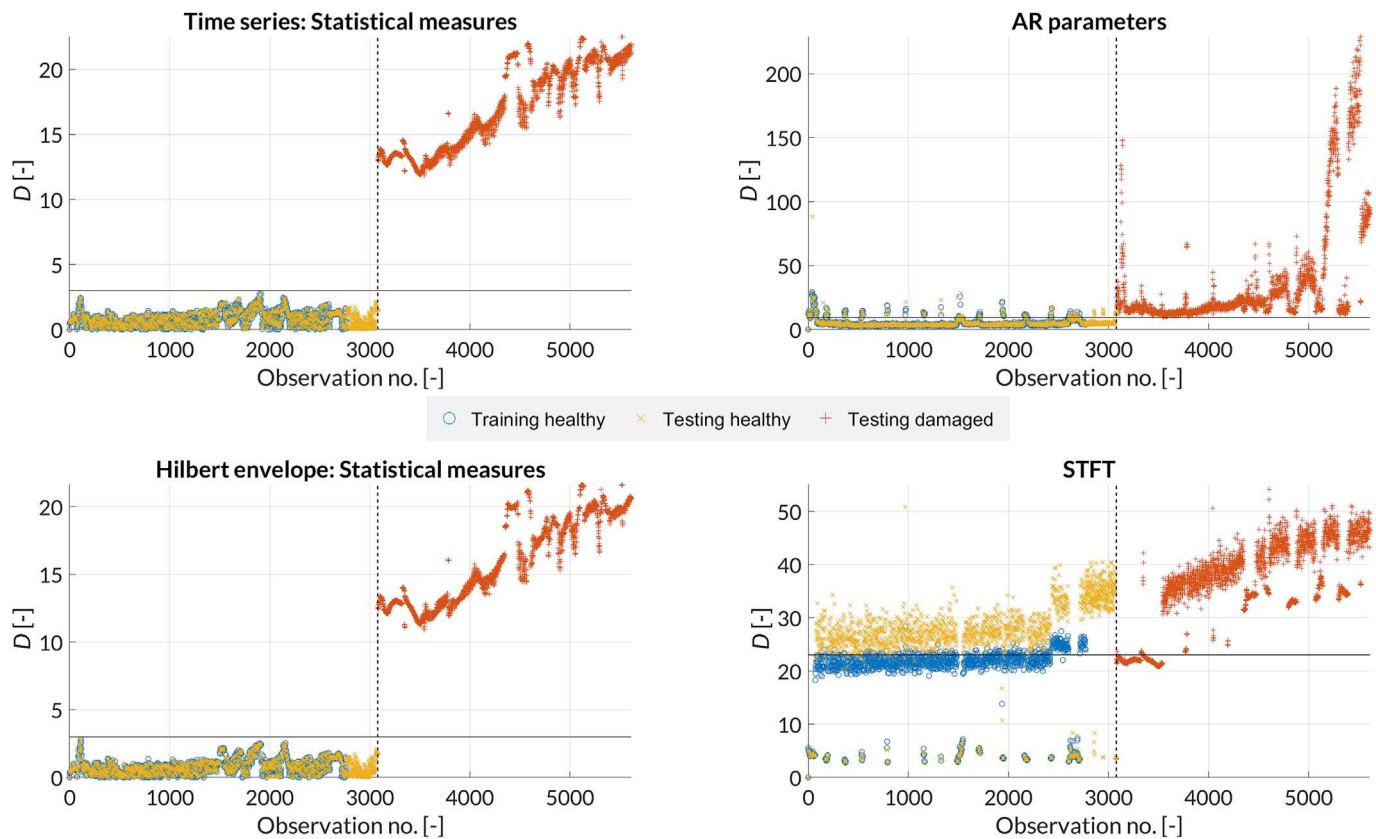
FIGURE 19 Damage indices D calculated using the four different presented features, based on accelerometer signals recorded with accelerometer 9 during active vibration excitation at frequency $f = 750$ Hz. Features are picked manually, and PCA is not performed.

TABLE 2 Classification accuracy [%], using features extracted with the different signal processing methods.

Accelerometer channel	1	2	3	4	6	7	8	9	10	11	12
Statistical measures	99.90	44.95	70.20	47.78	99.97	54.41	69.46	99.82	71.48	98.98	99.97
AR parameters	96.61	96.33	94.90	96.10	92.40	96.58	95.69	96.61	94.85	95.77	94.59
Hilbert envelope	99.87	51.25	79.80	60.82	99.95	64.49	88.19	99.57	77.45	98.47	99.87
STFT	99.87	96.33	95.74	86.12	99.92	82.27	88.83	99.90	95.80	99.97	99.64

Accelerometer placement on shear web: 1, 9, 11, and 12; spar cap: 8 and 10; shell: 2, 3, 4, 6, and 7.

For the features based on statistical measures of the time series data and Hilbert envelope, performance was generally mediocre when using data from accelerometers placed away from the shear web laminate. While a bandpass filter was applied to reduce operational noise, performance was generally found to be higher when using the STFT to extract the response at the frequency applied with the vibration shaker, removing the need for filtering the accelerometer data.

The application of single frequency input has the advantage of filtering being straightforward to apply for noise reduction, including the extraction of the frequency response from a specific STFT frequency line. Having shown that frequency domain methods yielded high performance in damage detection for the present study, applying e.g., several stepped consecutive frequencies, combined with using the STFT to extract features, may yield even higher performance and robustness for general application. The features presented in this paper are most likely not directly applicable for swept-sine signals, except for the AR parameters.

The proposed method for blade SHM, relying on active vibration excitation at specific frequencies, relies on the chosen excitation frequencies being sensitive to damage in the blade. Thus, using a higher number of excitation frequencies would yield higher robustness of the method. With excitation frequencies in the kHz range, the duration of application of the different vibration frequencies may be set shorter than used in this work, resulting in less data being necessary to process.

Using AR parameters as features, it was found that including accelerometer data sampled without active vibration excitation resulted in increased classification accuracy. Thus, there may be a potential for using AR parameters of medium-frequency vibration measurements, without the application of an active vibration excitation, for detection of changes in the structural state of wind turbine blades.

As an extension to the investigations performed in this work, which has focused on the time series response and frequency domain response of the recorded accelerometer data, the relative phase between the available sensor channels could be investigated as a possible feature for detection of initiation and progression of damage.

Regarding tracking of damage progression, it was found that the features did not necessarily increase monotonically with increasing damage severity. Since changes in local vibration response are used as the basis for the extracted features, changes in the features may be nonlinear. Thus, a damage index taking this into account may be useful for practical applications.

Features extracted from the data from some of the accelerometers exhibit clear separation between the healthy and damaged state, including progressive change in line with damage progression. On the other hand, some features only enabled separation of the healthy state and damaged state toward the highest damage severity observed in the blade test. Thus, the detectable damage size is shown to be dependent on the position of the accelerometer used for outlier analysis.

As shown with some of the presented outlier plots, the operational state may mask damage sensitivity of some of the features. Toward practical application in blades on operating turbines, steps should be taken to account for the operational state of the turbine, such that accurate classification of the health state can be obtained. As shown for some of the features, the use of PCA may be sufficient, whereas more effort will be required for other features. This behavior was also shown to be dependent on the sensor location, adding to the complexity of the problem. In general, a robust approach is deemed to be to account for operational effects through additional signal processing such as co-integration.

When comparing performance in classification accuracy for the data from two of the sensor channels, large differences were obtained between automated feature extraction through dimensionality reduction, compared to informed manual picking of damage-sensitive features. An important consideration in this context is the possible trade-off in computational time vs. classification accuracy. Automated feature extraction through PCA is computationally efficient and easy to implement, whereas manual feature picking requires an expert in the field to periodically inspect features and to determine if any of them exhibit changes due to a potential damage. The automated approach will generally be less costly to implement, especially if monitoring of blades for entire wind turbine parks is considered.

This work has used accelerometer measurements for detection changes in the local vibration response of the blade laminate, resulting from the initiation and progression of damage. Alternatively, the use of measurements from e.g., lasers or digital image correlation could be investigated.

For practical applications, the damage sensitivity of features may not be known beforehand. Ideally, several potentially damage-sensitive features are calculated, and dimensionality reduction, such as PCA, is conducted to reduce the feature space to the features which exhibit changes, possibly due to damage. As shown in this work, some features were found to be damage-sensitive, while others did not exhibit significant changes resulting from the initiation and development of damage. Using PCA, the damage-sensitive features were extracted, while the remaining features were rejected, resulting in increased performance in classification accuracy and reduced computational time. As an additional requirement for this process to be successful in detection of damage in blades on operating turbines, the effect of operational and environmental conditions, such as rotational speed of the turbine and ambient temperature, need to be filtered out, or features insensitive to changes in these conditions need to be selected.

5 | CONCLUSIONS

The present work investigated SHM of wind turbine blades using an active vibration monitoring system, applying sinusoidal signals with a Gaussian envelope, which yielded promising results toward application for blade SHM. A blade test was conducted, where a damage was introduced artificially, followed by progression during fatigue testing. Accelerometer data was collected at different parts of the blade laminate during active excitation with sinusoidal signals. Based on the collected data, different signal processing methods were used to extract potentially damage-sensitive features. The features were based on the Gaussian envelope of the applied vibration signals, enabling time-dependent changes in the amplitude response of the vibration signal. Features based on the statistical measures of the time series data and Hilbert envelope of the time series data yielded good performance in detection of initiation and progression of the shear web damage, provided that vibration data collected with an accelerometer on the shear web was used. Using data from accelerometers placed on the shell or spar cap laminate, operational noise present in the signal resulted in reduced performance, even though bandpass filtering was applied.

AR parameters did generally yield the highest performance in outlier detection, with classification accuracy being above 92% for the sensors placed furthest from the active vibration input. Using the STFT, the frequency line corresponding to the frequency of the applied sinusoidal signal was extracted, and the corresponding frequency response was used as a feature. This generally yielded good performance for every sensor channel in classification of observations in the healthy and damaged states, being attributed to the high signal-to-noise ratio at the frequency applied through the vibration shaker, while noise present at other frequencies did not affect this feature. Thus, the STFT and AR parameters, given active vibration input being applied, are deemed to be effective features for detection of changes in the local frequency response caused by damage.

Thus, detection of initiation and progression of damage in a wind turbine blade has been performed using a vibration shaker to apply an active vibration input and the vibration response from a single accelerometer. Furthermore, the proposed method is robust for application in the presence of two different operational states: stand-still and fatigue testing.

For future work, the application of consecutive stepped sinusoidal signals of shorter duration applied at a higher number of frequencies is suggested, using either the STFT or AR modeling to extract features. This is deemed to provide improved performance in detection of damage in wind turbine blades, while also providing increased robustness toward both sensor location and damage location. Generally, one of the next steps is to apply the findings from the present work and move toward application of an active vibration monitoring system on the blade of a modern, large-scale operating turbine to investigate how robust such a system is in the field.

CONFLICT OF INTEREST STATEMENT

The authors declare no potential conflict of interests.

PEER REVIEW

The peer review history for this article is available at https://www.webofscience.com/api/gateway/wos/peer-review/10.1002/we.2854.

DATA AVAILABILITY STATEMENT

Interested parties are welcome to contact the authors concerning sharing of the utilized data.

ORCID

M. A. Fremmelev https://orcid.org/0000-0003-4729-6569

K. Branner https://orcid.org/0000-0002-9601-6343

REFERENCES

1. Mackenzie W. Global offshore wind O&M spend to grow to 11 billion by 2028. 2019. https://www.woodmac.com/our-expertise/focus/Power-Renewables/global-offshore-wind-om-spend-to-grow-to-11-billion-by-2028/
2. Dao C, Kazemtabrizi B, Crabtree C. Wind turbine reliability data review and impacts on levelised cost of energy. *Wind Energy*. 2019;22(12):1848-1871.
3. Cevasco D, Koukoura S, Kolios AJ. Reliability, availability, maintainability data review for the identification of trends in offshore wind energy applications. *Renew Sustain Energy Rev*. 2021;136:110414. https://doi.org/10.1016/j.rser.2020.110414
4. McGugan M, Pereira G, Sorensen BF, Toftegaard H, Branner K. Damage tolerance and structural monitoring for wind turbine blades. *Philosoph Trans R Soc A: Math Phys Eng Sci*. 2015;373:20140077.
5. Chen X, Eder MA. A critical review of damage and failure of composite wind turbine blade structures. *IOP Conference Series: Materials Science and Engineering*, Vol. 942: IOP Publishing; 2020:12001.
6. Chen X. Fracture of wind turbine blades in operationPart I: A comprehensive forensic investigation. *Wind Energy*. 2018;21:1046-1063. https://doi.org/10.1002/we.2212
7. Ciang CC, Lee JR, Bang HJ. Structural health monitoring for a wind turbine system: A review of damage detection methods. *Measure Sci Technol*. 2008;19(12):122001.
8. Tchakoua P, Wamkeue R, Ouhrouche M, Slaoui-Hasnaoui F, Tameghe TA, Ekemb G. Wind turbine condition monitoring: State-of-the-art review, new trends, and future challenges. *Energies*. 2014;7(4):2595-2630.
9. Martinez-Luengo M, Kolios A, Wang L. Structural health monitoring of offshore wind turbines: A review through the Statistical Pattern Recognition Paradigm. *Renew Sustain Energy Rev*. 2016;64:91-105. https://doi.org/10.1016/j.rser.2016.05.085
10. Du Y, Zhou S, Jing X, Peng Y, Wu H, Kwok N. *Damage detection techniques for wind turbine blades: A review*, Vol. 141: Academic Press; 2020.
11. Malekimoghadam R, Krause S, Czichon S. *A critical review on the structural health monitoring methods of the composite wind turbine blades*, Vol. 110: Springer Singapore; 2021. https://doi.org/10.1007/978-981-15-9121-1_29
12. Civera M, Surace C. Non-destructive techniques for the condition and structural health monitoring of wind turbines: A literature review of the last 20 years. *Sensors*. 2022;22(4):1627.
13. Kaewniam P, Cao M, Alkayem NF, Li D, Manoach E. Recent advances in damage detection of wind turbine blades: A state-of-the-art review. *Renew Sustain Energy Rev*. 2022;167:112723. https://doi.org/10.1016/j.rser.2022.112723
14. Yang W, Peng Z, Wei K, Tian W. Structural health monitoring of composite wind turbine blades: Challenges, issues and potential solutions. *IET Renew Power Gen*. 2017;11:411-416. https://doi.org/10.1049/iet-rpg.2016.0087
15. Luczak MM, Peeters B, Manzato S, et al. Research sized wind turbine blade modal tests : Comparison of the impact excitation with shaker excitation. *Journal of Physics: Conference Series*, Vol. 1102: IOP Publishing; 2018:12022.
16. Lorenzo ED, Manzato S, Peeters B, et al. Modal analysis of wind turbine blades with different test setup configurations. *Topics in modal analysis & testing*, Vol. 8: Springer International Publishing; 2019:143-152.
17. Lorenzo E, Manzato S, Luczak M, Peeters B, Branner K. Strain-based operational modal analysis for wind turbine blades. In: Proceedings of the 8th International Operational Modal Analysis Conference IOMAC; 2019:12022.
18. Fremmelev MA, Ladpli P, Orlowitz E, Bernhammer LO, McGugan M, Branner K. Structural health monitoring of 52-meter wind turbine blade: Detection of damage propagation during fatigue testing. *Data-Centric Eng*. 2022;3:e22.

19. Chen X, Semenov S, McGugan M, et al. Fatigue testing of a 14.3 m composite blade embedded with artificial defects – Damage growth and structural health monitoring. *Composites Part A: Appl Sci Manufact*. 2021;140:106189. https://doi.org/10.1016/j.compositesa.2020.106189

20. Janeliukstis R, McGugan M. Control of damage-sensitive features for early failure prediction of wind turbine blades. *Struct Control Health Monit*. 2022; 29(1):e2852. https://doi.org/10.1002/stc.2852

21. Taylor SG, Jeong H, Jang JK, et al. Full-scale fatigue tests of CX-100 wind turbine blades. Part I: Testing. *Indust Commerc Appl Smart Struct Technol 2012*. 2012;8343:83430Q.

22. Taylor SG, Jeong H, Jang JK, et al. Full-scale fatigue tests of CX-100 wind turbine blades. Part II: Analysis. *Industr Commerc Appl Smart Struct Technol 2012*. 2012;8343:83430Q.

23. Dervilis N, Choi M, Antoniadou I, et al. Novelty detection applied to vibration data from a CX-100 wind turbine blade under fatigue loading. *J Phys: Conf Ser*. 2012;382:1-6.

24. Dervilis N, Choi M, Taylor SG, et al. On damage diagnosis for a wind turbine blade using pattern recognition. *J Sound Vibr*. 2014;333(6):1833-1850. https://doi.org/10.1016/j.jsv.2013.11.015

25. Dervilis N, Choi M, Antoniadou I, et al. Machine learning applications for a wind turbine blade under continuous fatigue loading. *Key Eng Mater*. 2014; 588:166-174.

26. Muñoz CQG, Marquez FPG, Crespo BH, Makaya K. Structural health monitoring for delamination detection and location in wind turbine blades employing guided waves. *Wind Energy*. 2019;22:698-711. https://doi.org/10.1002/we.2316

27. Worden K, Sohn H, Farrar CR. Novelty detection in a changing environment: Regression and interpolation approaches. *J Sound Vibr*. 2002;258(4): 741-761.

28. Avci O, Abdeljaber O, Kiranyaz S, Hussein M, Gabbouj M, Inman DJ. A review of vibration-based damage detection in civil structures: From traditional methods to machine learning and deep learning applications. *Mech Syst Signal Process*. 2021;147:107077.

29. Zhang C, Mousavi AA, Masri SF, Gholipour G, Yan K, Li X. Vibration feature extraction using signal processing techniques for structural health monitoring: A review. *Mech Syst Signal Process*. 2022;177:109175.

30. Jiménez AA, Zhang L, Muñoz CQG, Márquez FPG. Maintenance management based on machine learning and nonlinear features in wind turbines. *Renew Energy*. 2020;146:316-328.

31. Fitzgerald B, Arrigan J, Basu B. Damage detection in wind turbine blades using time-frequency analysis of vibration signals. In: The 2010 International Joint Conference on Neural Networks (IJCNN); 2010:1-5.

32. Tsai CS, Hsieh CT, Huang SJ. Enhancement of damage-detection of wind turbine blades via cwt-based approaches. *IEEE Trans Energy Conv*. 2006;21: 776-781.

33. Ulriksen MD, Tcherniak D, Kirkegaard PH, Damkilde L. Operational modal analysis and wavelet transformation for damage identification in wind turbine blades. *Struct Health Monit*. 2015;15(4):381-388.

34. Ulriksen MD, Skov JF, Kirkegaard PH, Damkilde L. Wavelet transformation for damage identification in wind turbine blades. *Struct Health Monit*. 2014;5:187-193. https://doi.org/10.1007/978-3-319-04570-2_21

35. Larsen GC, Berring P, Tcherniak D, Nielsen PH, Branner K. Effect of a damage to modal parameters of a wind turbine. In: Proceedings of the 7th European Workshop on Structural Health Monitoring; 2014:9.

36. Al-Khudairi O, Hadavinia H, Little C, Gillmore G, Greaves P, Dyer K. Full-scale fatigue testing of a wind turbine blade in flapwise direction and examining the effect of crack propagation on the blade performance. *Materials*. 2017;10(10):1152.

37. Li D, Ho SCM, Song G, Ren L, Li H. A review of damage detection methods for wind turbine blades; 2015.

38. Tcherniak D, Mølgaard LL. Vibration-based SHM system: Application to wind turbine blades. *J Phys: Conf Ser*. 2015;628(1):12072.

39. Ulriksen MD, Tcherniak D, Damkilde L. Damage detection in an operating Vestas V27 wind turbine blade by use of outlier analysis. In: 2015 IEEE Workshop on Environmental, Energy, and Structural Monitoring Systems, EESMS 2015 - Proceedings. Institute of Electrical and Electronics Engineers Inc.; 2015:50-55.

40. Tcherniak D, Mølgaard LL. Active vibration-based structural health monitoring system for wind turbine blade: Demonstration on an operating Vestas V27 wind turbine. *Struct Health Monit*. 2017;16(5):536-550.

41. García D, Tcherniak D. An experimental study on the data-driven structural health monitoring of large wind turbine blades using a single accelerometer and actuator. *Mech Syst Signal Process*. 2019;127:102-119.

42. Panagiotopoulos A, Dmitri T, Spilios FD. Damage detection on the blade of an operating wind turbine via a single vibration sensor and statistical time series methods: Exploring the performance limits of robust methods. *Struct Health Monit*. 2022;22(1):433-448.

43. Fremmelev MA, Ladpli P, Orlowitz E, Dervilis N, McGugan M, Branner K. A full-scale wind turbine blade monitoring campaign: Detection of damage initiation and progression using medium-frequency active vibrations; 2023.

44. Bishop CM. *Pattern Recognition and Machine Learning*: Springer; 2006.

45. MathWorks. Skewness. https://se.mathworks.com/help/stats/skewness.html

46. MathWorks. Kurtosis. https://se.mathworks.com/help/stats/kurtosis.html

47. Finotti RP, Cury AA, Barbosa FS. An SHM approach using machine learning and statistical indicators extracted from raw dynamic measurements. *Latin Am J Solids Struct*. 2019;16(2):1-7. https://doi.org/10.1590/1679-78254942

48. Makhoul J. Linear prediction: A tutorial review. *Proc IEEE*; 63(4):561-580.

49. Stoica PM. *Spectral analysis of signals*. New Jersey: Prentice Hall; 2004.

50. Marple SL. Computing the discrete-time analytic signal via fft. *IEEE Trans Signal Process*. 1999;47:2600-2603. https://doi.org/10.1109/78.782222

51. Goodwin MM. *The STFT, Sinusoidal Models, and Speech Modification: 229–258*: Springer Berlin Heidelberg; 2008.